DMD Fast Forward. Published on September 22, 2017 as DOI: 10.1124/dmd.117.077552
This article has not been copyedited and formatted. The final version may differ from this version.

Species-specific involvement of aldehyde oxidase and xanthine oxidase in the metabolism of the pyrimidine-containing $mGlu_5$ negative allosteric modulator VU0424238 (auglurant)

Rachel D. Crouch, Anna L. Blobaum, Andrew S. Felts, P. Jeffrey Conn and Craig W. Lindsley

Vanderbilt Center for Neuroscience Drug Discovery (RDC, ALB, ASF, PJC, CWL) Departments of Pharmacology (RDC, ALB, ASF, PJC, CWL) and Chemistry (CWL), Vanderbilt University School of Medicine, Nashville, TN 37232.

Running Title: Species-specific metabolism by molybdenum hydroxylases

Address correspondence to: Dr. Craig W. Lindsley, Vanderbilt Center for Neuroscience Drug Discovery, 2215 Garland Avenue, 1205 Light Hall, Nashville, TN 37232. Email: craig.lindsley@vanderbilt.edu

Text Pages: 26

Tables: 2

Figures: 9

References: 52

Words in Abstract: 249

Words in Introduction: 629

Words in Discussion: 1843

Abbreviations: AO, aldehyde oxidase; AOX1-4, aldehyde oxidase 1-4; CL_{int}, intrinsic clearance; CL_p, plasma clearance; DMPK, drug metabolism and pharmacokinetics; HPLC, high performance liquid chromatography; LC/MS, liquid chromatography mass spectrometry; LC/MS/MS, liquid chromatography tandem mass spectrometry; $mGlu_5$, metabotropic glutamate receptor subtype 5; MoCo, molybdenum cofactor; MRM, multiple reaction monitoring; NAM, negative allosteric modulator; P450, cytochrome P450; XIC, extracted ion chromatogram; XO, xanthine oxidase

Abstract

Aldehyde oxidase (AO) and xanthine oxidase (XO) are molybdo-flavoenzymes that catalyze oxidation of aromatic azaheterocycles. Differences in AO activity have been reported among various species including rat, human, and monkey. Herein we report a species difference in the enzymes responsible for metabolism of $mGlu_5$ NAM VU0424238 (VU238, auglurant). Hepatic S9 incubations with AO and XO specific inhibitors hydralazine and allopurinol indicated that rat and cynomolgus monkey both oxidized VU238 to the 6-oxopyrimidine metabolite M1 via an AO-mediated pathway, whereas secondary oxidation to the 2,6-dioxopyrimidine metabolite M2 was mediated predominantly by AO in monkey and XO in rat. Despite differences in enzymatic pathways, intrinsic clearance (CL_{int}) of M1 was similar between species (cynomolgus and rat CL_{int} = 2.00±0.040 and 2.19±0.201 μL/min/mg protein, respectively). Inhibitor studies in multiple species' S9 indicated oxidation of VU238 to M1 was mediated predominantly by AO in human, cynomolgus and rhesus monkey, rat, mouse, guinea pig, and minipig. Interestingly, oxidation of M1 to M2 was predominantly mediated by XO in rat and mouse and by AO in monkeys and guinea pig, while low turnover prevented enzyme phenotyping in human and minipig. Additionally, inhibitor experiments indicated oxidation at the 2-position of the pyrimidine ring of the known AO substrate, BIBX1382, was mediated by AO in all species, although production of this metabolite was comparatively low in rat and mouse. These data may suggest low reactivity of rat AO toward 2-oxidation of pyrimidine-containing compounds and highlight the importance of thoroughly characterizing AO-metabolized drug candidates in multiple preclinical species.

DMD Fast Forward. Published on September 22, 2017 as DOI: 10.1124/dmd.117.077552
This article has not been copyedited and formatted. The final version may differ from this version.

Introduction

Aldehyde oxidase (AO) and xanthine oxidase (XO) belong to a family of molybdo-flavoenzymes that catalyze the oxidation of nitrogen-containing aromatic heterocycles. Consequently, metabolism mediated by these enzymes, particularly AO, is now frequently encountered among drug discovery and development programs, as the inclusion of azaheterocycles in small molecule drug candidates has become a common tactic to evade cytochrome P450 metabolism or to engage particular targets such as kinases (Pryde et al., 2010). Species differences in the expression and activity of AO (Terao et al., 2016) present a challenge in predicting the metabolism and disposition of AO-metabolized compounds using traditional animal models, and consequently, several AO-metabolized drug candidates have failed during clinical trials (Dittrich et al., 2002; Diamond et al., 2010; Akabane et al., 2011; Infante et al., 2013; Lolkema et al., 2015; Jensen et al., 2017). In order to usefully employ preclinical animal models for the prediction of drug metabolism and disposition of AO substrates, a better understanding of the species differences surrounding this enzyme is needed.

Both AO and XO are cytosolic enzymes which function as a homodimer requiring a molybdenum-containing cofactor (MoCo) and FAD for catalytic activity (Pryde et al., 2010). Unlike AO, XO has the ability to interconvert between xanthine oxidase and xanthine dehydrogenase, whereas AO only exists as an oxidase (Pryde et al., 2010). While AO and XO share similar substrate specificities (both oxidize aromatic azaheterocycles on an electrophilic carbon atom adjacent to a nitrogen atom), AO metabolizes a broader array of substrates relative to XO, which has a general preference for purine/pyrimidine analogs (Kitamura et al., 2006; Pryde et al., 2010). Inhibitor specificities for the two enzymes differ as well, resulting in the ability to differentiate between AO and XO-mediated metabolism via the use of selective inhibitors such as

hydralazine (Johnson et al., 1985; Strelevitz et al., 2012) and allopurinol (Massey et al., 1970; Zientek and Youdim, 2015), respectively.

Some compounds can be substrates for both AO and XO, such as 6-deoxyacyclovir and 5-fluorouracil (Kitamura et al., 2006). In the case of 5-fluorouracil, oxidation by AO and XO occurs at the same site to produce the metabolite, 5-fluoro-6-oxouracil. Alternatively, 6-deoxyacyclovir is predominantly oxidized at the 6-position by XO and the 8-position by AO (Kitamura et al., 2006; Pryde et al., 2010). We previously reported on the role of AO and XO in the sequential metabolism of VU0409106, a negative allosteric modulator of the metabotropic glutamate receptor subtype 5 ($mGlu_5$ NAM) (Felts et al., 2013), in which case *in vitro* oxidation of the pyrimidine ring to the principle 6-oxopyrimidine metabolite was mediated by AO in human, monkey, and rat (Morrison et al., 2012). *In vitro* and *in vivo* experiments in Sprague-Dawley (SD) rat utilizing the XO inhibitor allopurinol indicated that a secondary oxidation, resulting in formation of a 2,6-dioxopyrimidine metabolite, was mediated by XO (Morrison et al., 2012; Crouch et al., 2016). These metabolites were also produced in cynomolgus monkey; however, experiments with allopurinol were not conducted.

We recently reported on the discovery of the novel $mGlu_5$ NAM VU0424238 (VU238, auglurant) as a potential clinical candidate for the treatment of a variety of psychiatric and neurodegenerative disorders (Felts et al., 2017). Similar to VU0409106, VU238 contains a pyrimidine head group which could be susceptible to oxidation by AO and/or XO. Accordingly, we found that VU238, like VU0409106, is also metabolized in an NADPH-independent manner to 6-oxopyrimidine (M1) and 2,6-dioxopyrimidine (M2) metabolites. During studies utilizing pharmacological inhibitors to evaluate the involvement of AO and XO in the formation of these metabolites, we discovered an apparent species difference in the primary enzyme responsible for

the formation of the 2,6-dioxopyrimidine metabolite, M2, between rat and cynomolgus monkey. A multispecies evaluation was conducted to further investigate species differences in the contributions of these two enzymes to the metabolism of VU238.

Materials and Methods

Materials.

N-(5-fluoropyridin-2-yl)-6-methyl-4-(pyrimidin-5-yloxy)picolinamide (VU0424238, VU238), N-(5-fluoropyridin-2-yl)-6-methyl-4-((pyrimidin-5-yl-2-d)oxy)picolinamide (VU6010180, VU180), and N-(5-fluoropyridin-2-yl)-6-methyl-4-((6-oxo-1,6-dihydropyrimidin-5-yl)oxy)picolinamide (VU0652922, VU922) were prepared and characterized by the Division of Medicinal Chemistry within the Vanderbilt Center for Neuroscience Drug Discovery. VU0424238 was prepared and characterized as previously described (Felts et al., 2017). Synthetic procedures for preparation of VU0652922 and VU6010180 are detailed below. Potassium phosphate, ammonium formate, formic acid, magnesium chloride, carbamazepine, hydralazine hydrochloride and allopurinol were purchased from Sigma-Aldrich (St. Louis, MO). BIBX1382 dihydrochloride was purchased from Tocris Bioscience (R&D Systems, Minneapolis, MN). 6-thioxanthine was purchased from Carbosynth (San Diego, CA) and 6-thiouric acid was purchased from Ark Pharm (Arlington Heights, IL). Pooled human hepatic S9 (150-donor, 50% male, 50% female, lot 38289), and pooled male Sprague-Dawley rat (n = 36, lot 4029004), pooled male cynomolgus monkey (n = 2, lot 5035001MUF), pooled male rhesus monkey (n = 6, lot 1), and pooled male CD-1 mouse (n = 170, lot 5023003) hepatic S9 were obtained from Corning Inc. (Tewksbury, MA). Pooled male Hartley guinea pig (n = 50, lot 0510020) hepatic S9 was purchased from XenoTech (Lenexa, KS). Pooled male Gottingen minipig (n = 7, lot KQQ) hepatic S9 and pooled female Sprague-Dawley rat (n = 6, lot BKM) and pooled female cynomolgus monkey hepatic S9 (n = 3, lot HWH) were purchased from BioreclamationIVT (Baltimore, MD). All solvents used for bioanalysis were purchased from Sigma-Aldrich or Fisher Scientific (Waltham, MA) and were of high-performance liquid chromatography (HPLC) grade.

DMD Fast Forward. Published on September 22, 2017 as DOI: 10.1124/dmd.117.077552
This article has not been copyedited and formatted. The final version may differ from this version.

Synthesis of N-(5-Fluoropyridin-2-yl)-6-methyl-4-((6-oxo-1,6-dihydropyrimidin-5-yl)oxy)picolinamide (M1, VU0652922).

4-(Benzyloxy)-5-bromopyrimidine (1). Benzyl alcohol (1.02 mL, 9.82 mmol, 2.00 eq) was dissolved in DMF (12 mL) and sodium hydride (248 mg, 9.82 mmol, 2.00 eq) was added. After 5 minutes 5-bromo-4-chloro-pyrimidine (950 mg, 4.91 mmol, 1.00 eq) was added as a solution in DMF (4 mL). The reaction was allowed to stir overnight and then quenched with a saturated solution of ammonium chloride. The mixture was diluted with ethyl acetate and washed with water (2x). The aqueous washes were back extracted with ethyl acetate and the combined organics were dried ($MgSO_4$), filtered and concentrated in vacuo. Purification using 0-20% hexanes/ethyl acetate afforded 1.04 g (80%) of the title compound as a clear oil: ES-MS $[M+1]^+$: 265.0.

4-(Benzyloxy)pyrimidin-5-ol (2). Compound 1 (797 mg, 3.01 mmol, 1.00 eq), potassium hydroxide (506 mg, 9.02 mmol, 3.00 eq), tris(dibenzylideneacetone)dipalladium(0) (165 mg, 0.180 mmol, 0.0600 eq), and 2-di-*tert*-butylphosphino-2′,4′,6′-triisopropylbiphenyl (153 mg, 0.361 mmol, 0.120 eq) were suspended in dioxane (7.5 mL) and water (7.5 mL) in a microwave vial and heated in a microwave reactor at 150 °C for 15 minutes. The reaction was neutralized to pH 4-5 with 2N HCl, extracted with ethyl acetate (1x) and 3:1 ($CHCl_3$/IPA) (2x). The combined organics were dried ($MgSO_4$), filtered and concentrated in vacuo. Purification using 0-5% DCM/MeOH afforded 368 mg (64%) of the title compound as an off-white solid: ES-MS $[M+1]^+$: 203.4.

4-((4-(Benzyloxy)pyrimidin-5-yl)oxy)-6-methylpicolinonitrile (3). Compound 2 (388 mg, 1.92 mmol, 1.00 eq), 4-chloro-6-methyl-pyridine-2-carbonitrile (293 mg, 1.92 mmol, 1.00 eq) and potassium carbonate (530 mg, 3.84 mmol, 2.00 eq) were suspended in DMF (5.8 mL) and heated overnight at 100 °C. *Note (Some amount of benzyl transfer is observed. NOESY NMR confirmed

DMD Fast Forward. Published on September 22, 2017 as DOI: 10.1124/dmd.117.077552
This article has not been copyedited and formatted. The final version may differ from this version.

the less polar product by LCMS to be the desired product). After cooling to room temperature the reaction was filtered and washed with ethyl acetate. The mixture was washed with water (2x) and the aqueous washes were back extracted with ethyl acetate. The combined organics were dried ($MgSO_4$), filtered and concentrated in vacuo. Purification using 0-40% hexanes/ethyl acetate afforded 247 mg (40%) of the title compound as a yellow solid: ES-MS $[M+1]^+$: 319.3.

4-((4-(Benzyloxy)pyrimidin-5-yl)oxy)-6-methylpicolinamide (4). Compound 3 (247 mg, 0.776 mmol, 1.00 eq) was dissolved in dioxane (3.9 mL) and 2N NaOH (1.55 mL, 3.10 mmol, 4.00 eq) was added. The reaction was heated at 60 °C for 6 hours at which point it was cooled and brought to pH 4-5 with 2N HCl. The mixture was concentrated to dryness, dissolved in 5% MeOH/DCM and filtered. The organics were concentrated to afford 233 mg (89%) of the title compound as a brown solid that was used without further purification: ES-MS $[M+1]^+$: 337.2.

4-((4-(Benzyloxy)pyrimidin-5-yl)oxy)-N-(5-fluoropyridin-2-yl)-6-methylpicolinamide (5). Compound 4 (233 mg, 0.693 mmol, 1.00 eq)), 2-bromo-5-fluoropyridine (183 mg, 1.04 mmol, 1.50 eq), palladium (II) acetate (7.78 mg, 0.0346 mmol, 0.0500 eq),4,5-bis(diphenylphosphino)-9,9-dimethylxanthene (40.1 mg, 0.0693 mmol, 0.100 eq) and sodium *tert*-butoxide (93.2 mg, 0.970 mmol, 1.40 eq) were dissolved in toluene (3.5 mL) and purged with nitrogen. The reaction was heated at 100 °C overnight, cooled and filtered over a celite pad. The pad was washed with 5% methanol/DCM and the combined organics were concentrated in vacuo. Purification using 0-40% hexanes/ethyl acetate afforded 156 mg (52%) of the title compound as a white solid: ES-MS $[M+1]^+$: 432.3.

N-(5-Fluoropyridin-2-yl)-6-methyl-4-((6-oxo-1,6-dihydropyrimidin-5-yl)oxy)picolinamide (M1-VU0652922). Compound 5 (156 mg, 0.362 mmol, 1.00 eq), was dissolved in chloroform (1.8 mL) and methanesulfonic acid (234 µL, 3.62 mmol, 10.0 eq) was

added. The reaction was stirred for 30 minutes and then neutralized with a saturated solution of sodium bicarbonate. The layers were separated and the aqueous phase was extracted with 3:1 $CHCl_3$/IPA (2x). The combined organics were dried ($MgSO_4$), filtered and concentrated in vacuo. Purification by reverse-phase chromatography afforded 92 mg (75%) of the title compound as a white solid: ^{1}H NMR (400 MHz, DMSO-d_6) δ 10.47 (s, 1H), 8.39 (d, J = 2.5 Hz, 1H), 8.29-8.24 (m, 2H), 8.14 (s, 1H), 7.86 (td, J = 2.6, 8.6 Hz, 1H), 7.43 (s, 1H), 7.19 (s, 1H), 2.56 (s, 3H); ES-MS $[M+1]^+$: 342.2.

Synthesis of N-(5-fluoropyridin-2-yl)-6-methyl-4-((pyrimidin-5-yl-2-d)oxy)picolinamide (VU6010180)

2-Bromo-5-((2-methoxyethoxy)methoxy)pyrimidine (6). 2-Bromo-5-hydroxypyrimidine (500 mg, 2.86 mmol, 1.00 eq), and *N*,*N*-diisopropylethylamine (1.49 mL, 8.57 mmol, 3.00 eq) were dissolved in DCM (7.2 mL) and cooled to 0 ºC. 2-Methoxyethoxymethyl chloride (653 µL, 5.71 mmol, 2.00 eq) was added as a solution in DCM (3.6 mL) and the reaction was allowed to warm to room temperature. After determination of completion by LCMS a saturated solution of sodium bicarbonate was added and the layers were separated. The aqueous phase was extracted with an additional portion of DCM and the combined organics were dried ($MgSO_4$), filtered and concentrated in vacuo. Purification using 0-15% hexanes/ethyl acetate afforded 484 mg (64%) of the title compound as a clear oil: ES-MS $[M+1]^+$: 263.0.

5-((2-Methoxyethoxy)methoxy)pyrimidine-2-d (7). Compound 6 (384 mg, 1.46 mmol, 1.00 eq), was dissolved in THF (3.6 mL) and diethyl ether (3.6 mL) and cooled to -100 °C using a bath of liquid nitrogen in ether. *n*-Butyllithium (1.4 M in hexanes) (1.15 mL, 1.61 mmol, 1.10 eq) was added dropwise keeping the temperature below -95 °C. After addition the reaction was stirred for 15 minutes at -100 °C and methanol-d_4 (1.19 mL, 29.2 mmol, 20.0 eq) was added. The reaction

was allowed to warm to room temperature and quenched with a saturated solution of ammonium chloride. The mixture was extracted with ethyl acetate (2x), dried ($MgSO_4$), filtered and concentrated in vacuo. Purification using 0-5% DCM/MeOH afforded 138 mg (51%) of the title compound as an off-white solid: ES-MS $[M+1]^+$: 186.2.

Pyrimidin-2-d-5-ol (8). Compound 7 (128 mg, 0.691 mmol, 1.00 eq) was dissolved in chloroform (3.5 mL) and methanesulfonic acid (449 µL, 6.91 mmol, 10.0 eq) was added. The reaction was stirred for 30 minutes and then neutralized with a saturated solution of sodium bicarbonate. The layers were separated and the aqueous phase was extracted with 3:1 $CHCl_3$/IPA (2x). The combined organics were dried ($MgSO_4$), filtered and concentrated in vacuo to afford 59 mg (88%) of the title compound as a yellow solid that was used without further purification: ES-MS $[M+1]^+$: 98.0. At this stage, remaining synthetic procedures for preparation of VU6010180 were carried out as described for VU0424238 (Felts et al., 2017).

Biotransformation in multispecies hepatic S9 fractions.

Substrates (5 or 20 µM) were incubated at 37 °C in borosilicate glass test tubes under ambient oxygenation for 60 minutes in a potassium phosphate-buffered reaction (100 mM, pH 7.4) containing hepatic S9 from human, mouse, rat, guinea pig, cynomolgus monkey, rhesus monkey, or minipig (2 or 5 mg/mL) and $MgCl_2$ (3 mM), with preincubation in the presence or absence of the aldehyde oxidase inhibitor hydralazine (50 µM) or the xanthine oxidase inhibitor allopurinol (100 µM). The total incubation volume was 0.5 mL. Reactions were initiated by the addition of substrate, terminated with the addition of 2 volumes of ice-cold acetonitrile, and subsequently centrifuged at 4000 rcf for 10 min. The resulting supernatants were dried under a stream of nitrogen and reconstituted in initial mobile phase in preparation for LC/MS analysis.

DMD Fast Forward. Published on September 22, 2017 as DOI: 10.1124/dmd.117.077552
This article has not been copyedited and formatted. The final version may differ from this version.

Intrinsic clearance (CL_{int}) in multispecies hepatic S9 fractions.

Substrates (1 μM) were incubated at 37 °C for 60 minutes in a potassium phosphate-buffered reaction (100 mM, pH 7.4) containing hepatic S9 from human, mouse, rat, guinea pig, cynomolgus monkey, rhesus monkey, or minipig (2.5 mg/mL) and $MgCl_2$ (3 mM). Reactions were initiated with addition of substrate, and at designated times (t = 0, 7, 15, 30, 45, and 60 min), aliquots were removed and precipitated with acetonitrile containing an internal standard (carbamazepine, 50 nM). The mixture was centrifuged at 4000 rcf for 5 min and resulting supernatants diluted with water in preparation for LC/MS/MS analysis of substrate depletion, by monitoring the analyte/internal standard peak area ratio. The intrinsic clearance (CL_{int}) was calculated from the elimination rate constant, *k*, which represents the slope determined from linear regression analysis of the natural log of the percent remaining substrate as a function of incubation time (Equation 1):

$$CL_{int}\ \ (mL/min/mg\ protein) = \frac{k\ min^{-1}}{2.5\ mg/mL} \quad (1)$$

A minimum of 15% substrate depletion by the terminal time point was considered a requirement to calculate CL_{int}. If this requirement was not met, an CL_{int} value was not reported. Data represent triplicate determinations and are reported as the mean ± standard deviation, obtained using GraphPad Prism version 5.04

Liquid chromatography-UV-mass spectrometry analysis.

LC/UV/MS analysis of substrates and metabolites generated *in vitro* was performed with an Agilent 1290 Infinity HPLC system coupled to a LTQ XL ion trap mass spectrometer (ThermoFisher Scientific, Waltham, MA). Analytes were separated by gradient elution using a Supelco Discovery C18 column (5 μm, 2.1 × 150 mm; Sigma-Aldrich, St. Louis, MO). Solvent A

was 10 mM (pH 4.1) ammonium formate, and solvent B was acetonitrile. The initial mobile phase was 85:15 A-B (v/v) for analysis of VU238, VU180, and VU922 and 90:10 A-B (v/v) for BIBX1382. Beginning at 5 min, the mobile phase was transitioned by linear gradient to 20:80 A-B over 20 min, held for two min, and transitioned back to starting conditions over two minutes for a total run time of 30 min. The flow rate was 0.400 ml/min. The HPLC eluent was first introduced into an Agilent 1290 diode array detector (254 nM) followed by electrospray ionization-assisted introduction into a LTQ XL ion trap mass spectrometer operated in positive ionization mode. Ionization was assisted with sheath and auxiliary gas (ultra-pure nitrogen) set at 50 and 20 psi, respectively. The electrospray voltage was set at 5 kV with the heated ion transfer capillary set at 350 °C and 31 V. Data were analyzed using Thermo XCalibur 2.2 software.

The extent of substrate depletion in S9 fractions was determined employing LC/MS/MS analysis with an electrospray ionization enabled Sciex API-4000 triple quadrupole instrument (Sciex, Foster City, CA) that was coupled to Agilent 1290 Infinity HPLC pumps (Agilent Technologies, Santa Clara, CA) and a CTC PAL autosampler (Leap Technologies, Carrboro, NC). Analytes were separated by gradient elution using a Kinetex C18 column (2.1 × 50 mm, 5 μm; Phenomenex, Torrance, CA) warmed to 40 °C. Mobile phase A was 0.1% formic acid in water (pH unadjusted) and mobile phase B was 0.1% formic acid in acetonitrile. The gradient started at 5% B after a 0.2-min hold and was linearly increased to 90% B over 1.0 min, held at 90% B for 0.4 min, and returned to 5% B in 0.1 min followed by a re-equilibration (0.3 min). The total run time was 2.0 min, and the HPLC flow rate was 0.5 mL/min. Mass spectral analyses were performed using multiple reaction monitoring (MRM), with transitions and voltages specific for each analyte using a Turbo Ion Spray source (source temp 500°C) in positive ionization mode (5.0 kV spray voltage). MRM transitions were the following: VU0424238 (*m/z* 326→186), VU0652922 (*m/z*

342→159), and carbamazepine (*m/z* 237 → 194). Data were analyzed using Sciex Analyst 1.5.1 software.

DMD Fast Forward. Published on September 22, 2017 as DOI: 10.1124/dmd.117.077552
This article has not been copyedited and formatted. The final version may differ from this version.

Results

Characterization of VU238 and NADPH-independent oxidative metabolites by LC/MS/MS.

VU0424238 (VU238) and the principle metabolites M1 and M2 produced *in vitro* in hepatic S9 of multiple species (Figure 1) were characterized by LC/MS/MS (Figure 2). Two major oxidative metabolites were produced in the absence of NADPH, and thus represent metabolism via NADPH-independent (e.g. non-P450) pathways. These two metabolites were also major metabolites observed in plasma of rats and monkeys administered VU238 *in vivo* (data not shown). A minor metabolite likely representing the carboxylic acid product of amide hydrolysis was also detected in extracts from NADPH-independent S9 experiments, and additional minor oxidative metabolites were detected in hepatic S9 extracts from incubations conducted in the presence of NADPH (data not shown). The following experiments presented herein focus solely on the NADPH-independent metabolism of VU238.

VU0424238. The protonated molecular ion $[M + H]^+$ for VU238 was observed at *m/z* 326 with a retention time of 13.5 min. MS/MS fragmentation of VU238 produced predominant fragment ions at *m/z* 308, corresponding to a loss of water, *m/z* 214, corresponding to fragmentation of the amide bond, and *m/z* 186, corresponding to fragmentation adjacent to the amide bond, liberating the biaryl ether moiety (Figure 2A). A fragment ion at *m/z* 159 corresponds to the loss of HCN from the fragment ion at *m/z* 186.

VU0652922 (M1). The protonated molecular ion $[M + H]^+$ for the major oxidative metabolite produced in S9 of all species, M1, was observed at *m/z* 342 with a retention time of 11.1 min. Fragment ions produced at *m/z* 324, 230, 202, and 175 each correspond to the aforementioned fragment ions produced by VU238 with a mass shift of +16 Da (Figure 2B). The fragment ion at *m/z* 159 corresponds to the loss of CHNO from the fragment ion at *m/z* 202.

DMD Fast Forward. Published on September 22, 2017 as DOI: 10.1124/dmd.117.077552
This article has not been copyedited and formatted. The final version may differ from this version.

Structural assignment of M1 was confirmed by LC/MS/MS analysis of a synthetic standard (VU0652922, VU922), which revealed an MS/MS fragmentation pattern and retention time consistent with that observed for M1 from S9 extracts (data not shown). Refer to Supplemental Figure 1 for the NMR spectra of VU922.

M2. A metabolite with a mass shift of +32 Da over the protonated molecular ion $[M + H]^+$ of the parent VU238 was observed at *m/z* 358 with a retention time of 10.8 min. Fragment ions produced at *m/z* 340, 246, 218, and 191 each correspond to the aforementioned fragment ions produced by VU238 with a mass shift of +32 Da (Figure 2C). The fragment ion at *m/z* 175 corresponds to the loss of CHNO from the fragment ion at *m/z* 218. The assignment of the secondary oxidation site to the 2-position of the pyrimidine ring was supported by LC/MS/MS analysis of metabolites generated during hepatic S9 incubation of a deuterated analog of VU238 (VU6010180), where a deuterium has replaced the hydrogen atom in the 2-position of the pyrimidine ring. The results of this experiment are described below.

Incubation of VU6010180 in cynomolgus monkey hepatic S9.

The mechanism for oxidation of nitrogen-containing heterocycles by the molybdenum-containing hydroxylases AO and XO proceeds via hydride displacement from the carbon (adjacent to a nitrogen) being oxidized (Alfaro and Jones, 2008). Therefore, the hydrogen atom located at the site of oxidation is removed during the course of oxidation. Accordingly, replacement of the hydrogen in the 2-position of the pyrimidine ring of VU238 with a deuterium (VU6010180, VU180) resulted in a kinetic deuterium isotope effect on the formation of M2, where the turnover of M1 to M2 was reduced in S9 incubations with VU180 relative to those with VU238 (Figure 3A). In addition, while the presence of the deuterium label in VU180 and its respective M1 metabolite was evidenced by production of a protonated molecular ion $[M + H]^+$ differing from

DMD Fast Forward. Published on September 22, 2017 as DOI: 10.1124/dmd.117.077552
This article has not been copyedited and formatted. The final version may differ from this version.

VU238 and its M1 metabolite by +1 Da, respectively (Figure 3B and C), the $[M + H]^+$ produced by M2 was the same (*m/z* 358) in extracts from incubations with either VU238 or VU180, indicating the deuterium label was lost during M2 formation (Figure 3D). Together these data support assignment of the secondary oxidation to the 2-position of the pyrimidine ring.

Hepatic S9 incubation of VU238 and VU922 with AO and XO inhibitors.

The NADPH-independent formation of M1 and M2 in hepatic S9 incubations, in conjunction with oxidation on the pyrimidine ring, indicated the likely involvement of AO or XO in the formation of these metabolites. In order to determine whether AO or XO contributes to formation of M1 and M2, VU238 was incubated in male cynomolgus monkey hepatic S9 in the presence or absence of the AO inhibitor hydralazine or the XO inhibitor allopurinol. Incubation with allopurinol resulted in little-to-no inhibition of M1 or M2 formation, while incubation with hydralazine inhibited formation of both M1 and M2 in cynomolgus monkey S9 (Figure 4A). Hydralazine also inhibited formation of M1 and M2 in male rat hepatic S9 (Figure 4B). However, while allopurinol had no effect on M1 formation in rat S9, formation of M2 was attenuated (Figure 4B). These data suggest that XO plays a major role in the conversion of M1 to M2 in rat, but not in cynomolgus monkey. Furthermore, incubation of synthetically prepared M1 (VU922) with allopurinol or hydralazine in cynomolgus monkey hepatic S9 revealed that hydralazine inhibited formation of M2, while allopurinol had little effect (Figure 5A). Conversely, in rat S9, allopurinol attenuated formation of M2, while hydralazine had little effect (Figure 5B).

Multispecies metabolism of VU238 and VU922 in hepatic S9.

The apparent species difference in metabolism of M1 to M2 between rat and cynomolgus monkey prompted a multispecies evaluation to determine the potential role of AO and XO in VU238 metabolism by several species commonly employed in DMPK studies. In addition to male

rat and cynomolgus monkey, VU238 was incubated with hepatic S9 of human (mixed gender), and male rhesus monkey, mouse, guinea pig, and minipig. The relative abundance of M1 and M2 differed across species, with the greatest turnover of VU238 to M1 occurring in rat and cynomolgus monkey. M1 and M2 were detected in S9 extracts of all species except human and minipig, which did not contain M2 at detectable levels (Figure 6A). However, trace levels of M2 were detected in human and minipig S9 extracts from direct incubations with M1 (VU922) (Figure 6B), indicating these species are capable of producing this metabolite. In general, while species exhibiting relatively high turnover of VU238 to M1 also exhibited relatively high turnover of VU922 to M2, minipig exhibited extensive turnover of VU238 to M1, but very low turnover of VU922 to M2.

Multispecies S9 incubations were also conducted with allopurinol and hydralazine. These data are summarized in Table 1, where designations of "AO" or "XO" indicate that formation of the metabolite was inhibited predominantly by hydralazine or allopurinol, respectively. Conversion of VU238 to M1 was inhibited by hydralazine in all species, whereas conversion of M1 to M2 was inhibited by hydralazine in monkeys and guinea pig, but not in rat and mouse, in which cases allopurinol inhibited conversion of M1 to M2 (Table 1). Extracted ion chromatograms for these experiments are illustrated in Supplemental Figures 2 and 3 along with peak area percentages in Supplemental Table 1. The predominant metabolic pathway mediating conversion of M1 to M2 in human and minipig could not be determined from the present experiments. Specifically, extracts of S9 incubations with hydralazine contained a trace analyte possessing a protonated molecular ion $[M + H]^+$ at *m/z* 357 and a retention time similar to that of M2 (10.8 min), which interfered with quantitation of M2 (*m/z* 358) in hydralazine-containing extracts. Due to low turnover of M1 to M2 in human and minipig S9, M2 could not be distinguished from the

interfering analyte in extracts of incubations with hydralazine (Supplemental Figures 3A and 3E). Although the identity of this analyte is unknown, it was also present in extracts of S9 incubations containing only hydralazine (no substrate), which suggests that it is unrelated to VU238 or its metabolites. While a conclusion regarding the enzymatic pathway mediating conversion of M1 to M2 in human and minipig cannot be reliably obtained from the current data, inhibition of M2 formation was not observed in the presence of allopurinol, indicating that XO may not substantially contribute.

Barr et al. previously reported that human liver fractions may lack XO activity due to the inclusion of allopurinol in liver perfusion solutions used during the process of harvesting human livers (Barr et al., 2014). In order to confirm XO activity in hepatic S9 fractions of human as well as the other species examined herein, the exemplary XO substrate 6-thioxanthine (6-TX) was incubated with hepatic S9 in the presence and absence of allopurinol or hydralazine, and the formation of 6-thiouric acid (6-TUA) was monitored. Formation of 6-TUA was observed in S9 of all species and likewise was inhibited by allopurinol in S9 of all species (Supplemental Figure 5, Supplemental Table 2), confirming the presence of XO activity. While human and minipig demonstrated low turnover, all other species exhibited extensive metabolism of 6-TX to 6-TUA. Formation of 6-TUA in S9 of monkeys and guinea pigs was mildly inhibited by hydralazine, indicating the possibility that AO may contribute to metabolism of 6-TX in these species.

Sex differences in AO activity have been reported in some species (Beedham, 1985; Klecker et al., 2006; Akabane et al., 2011; Dalvie et al., 2013), including rat and cynomolgus monkey, while reports indicate human AO exhibits no sex differences in activity (Al-Salmy, 2001; Klecker et al., 2006; Dalvie et al., 2013; Hutzler et al., 2014b). To explore potential sex differences in rat and cynomolgus monkey, we conducted incubations of VU238 and VU922 in the presence

and absence of inhibitors in female rat and cynomolgus monkey S9. Turnover of both VU238 to M1 (Figure 7) and VU922 to M2 (Figure 8) were low in both female cynomolgus and rat S9 when compared to incubations with male S9. Accordingly, M2 was not detected in female cynomolgus and rat S9 extracts from incubations with VU238, but only those with direct incubation of VU922. However, inhibition patterns between male and female cynomolgus and rat S9 experiments were similar, where conversion of VU238 to M1 was inhibited by hydralazine in both species/sexes. Likewise, conversion of M1 to M2 was inhibited by allopurinol in incubations of M1 (VU922) with both female and male rat S9. However, low turnover and the presence of the previously described interfering analyte in hydralazine-containing extracts, which eluted at the same retention time as M2, prevented a conclusive result concerning the inhibitory activities of allopurinol versus hydralazine toward formation of M2 in female cynomolgus monkey S9 incubations.

Multispecies intrinsic clearance (CL_{int}) of VU238 and VU922 in hepatic S9.

We also evaluated the *in vitro* clearance of VU238 and VU922 in hepatic S9 of multiple species (male S9, with the exception of human which was mixed gender). Experiments were conducted in the absence of NADPH, and therefore, the values are expected to predominantly represent clearance resulting from hepatic AO/XO-mediated oxidation (though it is possible that a small contribution resulted from amide hydrolysis). These data are summarized in Table 2. CL_{int} of VU238 was highest in cynomolgus monkey and rat, lowest in human and guinea pig, with rhesus monkey, mouse, and minipig falling in the middle range. CL_{int} of VU922 was low in all species, with turnover rates so low in human, mouse, and minipig S9 that CL_{int} could not be determined in these species. Overall, these data were consistent with the relative metabolite formation we observed across species in metabolism experiments with hepatic S9.

Multispecies metabolism of BIBX1382 in hepatic S9.

BIBX1382 is another pyrimidine-containing compound reported to be oxidized at the 2-position of one of its two pyrimidine rings by human and monkey AO (Hutzler et al., 2012; Hutzler et al., 2014a). In addition to this primary oxidation, a secondary NADPH-independent oxidation has been reported (Hutzler et al., 2014a). This secondary oxidation likely occurs on BIBX1382's pyrimido-pyrimidine core but has not been confirmed. BIBX1382 is also reportedly cleared much more rapidly in human and monkey relative to rat and mouse (Dittrich et al., 2002; Hutzler et al., 2014a). These differences were noted in the *in vitro* CL_{int} of BIBX1382 as well (Hutzler et al., 2014a; Crouch et al., 2017). In order to determine if the NADPH-independent metabolism of BIBX1382 is also inhibited by hydralazine and allopurinol in a species-specific manner (as was observed with the metabolism of VU238/VU922), BIBX1382 was incubated in hepatic S9 of multiple species in the presence and absence of inhibitors. Extracted ion chromatograms for these experiments are depicted in Figure 9A-B for cynomolgus monkey and rat and in Supplemental Figure 4 for all other species. These data are summarized in Figure 9C.

In accordance with the species differences in clearance rates previously reported for BIBX1382, we observed species differences in the turnover of BIBX1382 to M1b (primary oxidative metabolite), as well as in the turnover of M1b to M2b (secondary oxidative metabolite). BIBX1382 was extensively converted to M1b in all species except rat and mouse, which demonstrated poor turnover to M1b (Figure 9, Supplemental Figure 4). Unlike our observations of species differences in the inhibitory activities of hydralazine and allopurinol on the conversion of VU922 to M2, we observed no species differences in the inhibition of BIBX1382 conversion to M1b. Formation of BIBX1382 metabolites M1b and M2b was inhibited by hydralazine in incubations of BIBX1382 with S9 of all species, whereas minimal inhibition resulted from the

presence of allopurinol (Figure 9, Supplemental Figure 4, Supplemental Table 1). Inhibitory activity on the formation of M2b was not evaluated via direct incubation of M1b, and thus, the contributions of AO and XO toward formation of this secondary metabolite were not determined. However, the minimal impact of allopurinol on M2b levels in incubations with BIBX1382 suggests that XO may only play a small role (if any) in the formation of M2b in any of the species evaluated.

DMD Fast Forward. Published on September 22, 2017 as DOI: 10.1124/dmd.117.077552
This article has not been copyedited and formatted. The final version may differ from this version.

Discussion

VU238 was under development by our group as a candidate drug to treat various neurological disorders, such as Alzheimer's disease, pain, fragile X syndrome, levodopa-induced dyskinesia in Parkinson's disease, depression, addiction, and anxiety, by specifically targeting the $mGlu_5$ receptor via an allosteric site (Felts et al., 2017). Brain-penetrant with good oral bioavailability and low clearance in rat and monkey (F = 0.53 and 0.44, respectively; CL_p = 19.3 and 15.5 mL/min/kg, respectively), VU238 was found to potently and selectively inhibit $mGlu_5$ *in vitro* (human $mGlu_5$ IC_{50} = 14 nM) and demonstrate efficacy in rodent models of anxiety and depression (Felts et al., 2017). Unfortunately, advancement of VU238 into first-in-human studies was halted after a 28-day toxicological assessment indicated species-specific toxicities in cynomolgus monkeys, which were not observed in rats. While mechanisms responsible for these toxicities are currently under investigation, they are suspected to be metabolism-related. Consequently, utilizing the AO and XO inhibitors hydralazine and allopurinol, we uncovered an apparent species difference between rat and monkey in the enzymes involved in formation of the 2,6-dioxopyrimidine metabolite (M2) of VU238. Given these observations, it is possible that species differences in the involvement of AO and XO in VU238 metabolism could play a role in the observed monkey-specific toxicity.

Experiments with allopurinol and hydralazine indicated little role (if any) for AO in the formation of M2 in rat and mouse, which could be attributed to species differences in hepatic AO expression. Human, monkey, and guinea pig, for example, express only a single liver isoform, AOX1, while mouse and rat express two, AOX1 and AOX3 (Terao et al., 2016). Furthermore, the AOX3 isoform is present in higher quantities than AOX1 in mouse hepatic tissue, and computational and site-directed mutagenesis studies suggest differences in the substrate

specificities of these two isoforms (Terao et al., 2016) (Coelho et al., 2012; Mahro et al., 2013)(Cerqueira et al., 2015). Recently, a direct comparison of mouse AOX1 and AOX3 revealed substantial differences in the kinetic parameters of six substrates between the two isoforms (Kucukgoze et al., 2017). Accordingly, because our studies indicate that M1 is converted to M2 predominantly by XO rather than AO in rat and mouse, it is possible that M1 (VU922) is a poor substrate for AOX3 relative to AOX1. However, because we also observed low turnover of M1 to M2 in human S9 (Supplemental Figure 3A), structural differences in AOX1 across species, among other factors, may contribute to the observed species differences.

While rat has been generally labeled as a species with low AO activity, our data reiterate observations in the literature indicating that relative AO activity in rat versus other species is substrate-dependent (Beedham et al., 1987; Kawashima et al., 1999; Kitamura et al., 1999; Itoh et al., 2006; Dalvie et al., 2013; Crouch et al., 2017). AO-mediated oxidation of zaleplon, for example, is reportedly higher in cynomolgus monkey versus Sprague-Dawley rat (Kawashima et al., 1999), while the converse has been reported for zoniporide (Dalvie et al., 2013). Presently, we found that the CL_{int} of VU238 and its metabolism to M1 in hepatic S9 was similar between rat and cynomolgus monkey, while the CL_{int} and metabolism of BIBX1382 to M1b was much lower in rat versus cynomolgus monkey, consistent with prior reports of *in vivo* and *in vitro* BIBX1382 clearance (Dittrich et al., 2002; Hutzler et al., 2014a)(Crouch et al., 2017). Despite similar AO–mediated conversion of VU238 to M1 between cynomolgus monkey and rat, AO appeared to play little role in the secondary oxidation of M1 (VU922) to M2 in rat. Notably, conversion of BIBX1382 to M1b and of VU922 to M2 both proceed via oxidation at the 2-position of a pyrimidine ring. Itoh et al. previously reported decreased AO-mediated 2-oxidation of the pyrimidine ring of RS-8359 in rat relative to monkey (Itoh et al., 2006). These data together may

indicate that rat AO has low reactivity toward 2-oxidation of a pyrimidine versus monkey. This, of course, does not take into account other structural components outside of the pyrimidine ring which may influence metabolism at the 2-position. Rashidi et al. previously demonstrated that both AO and XO contribute to 6-oxidation of the guanine derivative 6-deoxypenciclovir in rat liver fractions, whereas the oxidation was found to be exclusively mediated by AO in human, guinea pig, and rabbit (Rashidi et al., 1997). The contribution of XO, however, was primarily evident in rats reported to be "AO deficient." Alternatively, 6-oxidation of famciclovir (diacetyl ester of 6-deoxypenciclovir) was found to be mediated exclusively by AO in all species (Rashidi et al., 1997). Investigations into factors influencing substrate specificity/reactivity of AO have been conducted (Vila et al., 2004; Fukiya et al., 2010; Pryde et al., 2010; Coelho et al., 2012; Dalvie et al., 2012; Jones and Korzekwa, 2013; Cerqueira et al., 2015; Choughule et al., 2015; Coelho et al., 2015; Terao et al., 2016; Lepri et al., 2017; Xu et al., 2017), though most focus primarily on human or mouse AO. Furthermore, following evaluation of 198 aza-aromatic compounds for susceptibility toward metabolism by human AO, Lepri et al. concluded that AO substrate prediction is not a simple task (Lepri et al., 2017).

Interestingly, while XO appears to metabolize VU922 to M2 in rat, we observed essentially complete inhibition of M2 formation by hydralazine in cynomolgus monkey S9 and minimal attenuation by allopurinol, suggesting that XO plays a very minor role, if any, in cynomolgus monkey. Sharma et al. previously reported a species difference in the oxidation of a quinoxaline derivative by plasma xanthine oxidase, where the compound was extensively metabolized in rodent plasma (rat, mouse, and guinea pig), but was stable in plasma of dog, monkey, and human (Sharma et al., 2011). Although our studies were conducted in hepatic S9, thus representing hepatic XO activity, a similar result was obtained in which formation of M2 was inhibited by allopurinol

in rat (and mouse) S9, but was minimally affected by the XO inhibitor in monkey S9. Interestingly, experiments with guinea pig S9 indicated that conversion of M1 to M2 proceeds via an AO-mediated pathway similar to monkey, with hydralazine mediating nearly complete inhibition. This observation is not altogether surprising, given the reported expression of only AOX1 (absence of AOX3) in both guinea pigs and monkeys (Garattini and Terao, 2012); although we might have anticipated more involvement from XO in guinea pig based on the observations reported by Sharma et al. Notably, M2 was not detected in extracts obtained from *in vitro* incubations of VU922 (20 μM substrate, incubated for 90 minutes at 37 ^{o} C) in rat or cynomolgus monkey plasma (data not shown), suggesting VU922 is not metabolized by plasma XO in either species. Importantly, 6-TX was metabolized to 6-TUA (inhibited by allopurinol) in S9 of all species, demonstrating that XO activity was present. However, human and minipig S9 fractions exhibited low turnover of 6-TX relative to the other species. While use of allopurinol during the harvesting of human livers may explain this observation in human S9 (Barr et al., 2014), vendors that supplied S9 fractions used in these studies reported that animal livers are harvested without the use of allopurinol. It is unclear if low XO activity contributed to the low turnover of VU922 to M2 in human and minipig S9.

Along with species differences in AO activity, substrate-specific sex differences have also been observed in certain species (Beedham, 1985; Klecker et al., 2006; Akabane et al., 2011; Dalvie et al., 2013). In addition to evaluating VU238/VU922 metabolism in male hepatic S9 of multiple species, we also evaluated metabolism in female rat and cynomolgus monkey S9. While turnover in female S9 was low compared to male S9 in both species, the involvement of AO and XO appeared to be the same regardless of sex (the enzymatic pathway of VU922 to M2 could not be confirmed from the present data in female cynomolgus monkey, though it would appear that

the reaction was minimally affected by allopurinol). Variability in AO activity has been observed *in vitro*, particularly with regard to human *in vitro* preparations (Fu et al., 2013; Hutzler et al., 2014b), and differences have been noted in AO activity when comparing cytosol and S9 obtained from different vendors (Zientek and Youdim, 2015). Consequently, male and female S9 fractions used in our experiments were obtained from different vendors, which could have influenced the activity displayed in these studies. Interestingly, while the AO-mediated turnover of VU238 to M1 was much lower in female rat S9 versus male (female M1:VU238 ratio = 0.03; male M1:VU238 ratio = 1.1), the difference in XO-mediated turnover of VU922 to M2 between male and female rat S9 incubations was not nearly as dramatic (female M2:VU922 ratio = 0.2; male M2:VU922 ratio = 0.4). These data are consistent with reports of sex-dependent xanthine oxidase activity in Sprague-Dawley rats, indicating males exhibit greater activity than females (Levinson and Chalker, 1980; Decker and Levinson, 1982). As prior reports indicate sex differences in AO activity are likely substrate-, species-, and even strain-dependent (Beedham, 1985; Klecker et al., 2006; Akabane et al., 2011; Dalvie et al., 2013), sex may be an important consideration when selecting species for toxicological evaluations of AO/XO substrates.

Our observations highlight an additional complication in the use of animal models for understanding human metabolism and disposition of AO substrates. While two species may exhibit similar AO activity toward the parent compound, profound species differences may still exist in secondary AO-mediated metabolism of a primary metabolite. Consequently, following identification of an AO- (or XO-) mediated pathway in one species, caution should be taken not to assign the same pathway to other species without confirmation, as misidentification of the responsible enzyme could result in unexpected pharmacokinetic drug-drug interactions. Furthermore, potential differences in extra-hepatic expression of AO (Terao et al., 2016) versus

XO (Pritsos, 2000; Agarwal et al., 2011) may result in unanticipated metabolite exposures *in vivo* if the correct enzyme has not been identified. As metabolites generated by AO have been associated with toxicities related to poor solubility (Smeland et al., 1996; Infante et al., 2013; Lolkema et al., 2015), unanticipated metabolite exposures could also lead to unanticipated toxicity *in vivo*.

In conclusion, we have demonstrated a species difference in the secondary metabolism of VU238, in which the primary oxidative pathway was determined to be mediated by AO in human, cynomolgus and rhesus monkey, rat, mouse, guinea pig, and minipig, and the subsequent oxidation was found to be predominantly mediated by XO in rat and mouse and by AO in monkeys and guinea pig. These data will be important to consider when AO- or XO-mediated metabolism is suspected in order to avoid incorrect assignment of a metabolism pathway due to differences across species. As literature reports continue to indicate that species differences in AO activity are substrate-dependent, selection of preclinical species for prediction of human PK and *in vivo* toxicology should be customized to each newly identified AO substrate (Crouch et al., 2017). Continued investigation into species differences surrounding AO metabolism (e.g. substrate specificity, expression and regulation, etc.) will be useful in guiding substrate-specific experiments to determine the most suitable species.

Authorship Contributions

Participated in research design: Crouch, Blobaum, Felts, Lindsley

Conducted experiments: Crouch

Contributed new reagents or analytical tools: Felts

Performed data analysis: Crouch, Felts

Wrote or contributed to the writing of the manuscript: Crouch, Blobaum, Felts, Conn, Lindsley

References

Agarwal A, Banerjee A, and Banerjee UC (2011) Xanthine oxidoreductase: a journey from purine metabolism to cardiovascular excitation-contraction coupling. *Critical reviews in biotechnology* **31:**264-280.

Akabane T, Tanaka K, Irie M, Terashita S, and Teramura T (2011) Case report of extensive metabolism by aldehyde oxidase in humans: Pharmacokinetics and metabolite profile of FK3453 in rats, dogs, and humans. *Xenobiotica* **41:**372-384.

Al-Salmy HS (2001) Individual variation in hepatic aldehyde oxidase activity. *IUBMB Life* **51:**249-253.

Alfaro JF and Jones JP (2008) Studies on the mechanism of aldehyde oxidase and xanthine oxidase. *J Org Chem* **73:**9469-9472.

Barr JT, Choughule KV, Nepal S, Wong T, Chaudhry AS, Joswig-Jones CA, Zientek M, Strom SC, Schuetz EG, Thummel KE, and Jones JP (2014) Why do most human liver cytosol preparations lack xanthine oxidase activity? *Drug Metab Dispos* **42:**695-699.

Beedham C (1985) Molybdenum hydroxylases as drug-metabolizing enzymes. *Drug Metab Rev* **16:**119-156.

Beedham C, Bruce SE, Critchley DJ, al-Tayib Y, and Rance DJ (1987) Species variation in hepatic aldehyde oxidase activity. *Eur J Drug Metab Pharmacokinet* **12:**307-310.

Cerqueira NM, Coelho C, Bras NF, Fernandes PA, Garattini E, Terao M, Romao MJ, and Ramos MJ (2015) Insights into the structural determinants of substrate specificity and activity in

mouse aldehyde oxidases. *Journal of biological inorganic chemistry : JBIC : a publication of the Society of Biological Inorganic Chemistry* **20:**209-217.

Choughule KV, Joswig-Jones CA, and Jones JP (2015) Interspecies differences in the metabolism of methotrexate: An insight into the active site differences between human and rabbit aldehyde oxidase. *Biochem Pharmacol* **96:**288-295.

Coelho C, Foti A, Hartmann T, Santos-Silva T, Leimkuhler S, and Romao MJ (2015) Structural insights into xenobiotic and inhibitor binding to human aldehyde oxidase. *Nat Chem Biol* **11:**779-783.

Coelho C, Mahro M, Trincao J, Carvalho AT, Ramos MJ, Terao M, Garattini E, Leimkuhler S, and Romao MJ (2012) The first mammalian aldehyde oxidase crystal structure: insights into substrate specificity. *J Biol Chem* **287:**40690-40702.

Crouch RD, Hutzler JM, and Daniels JS (2017) A novel in vitro allometric scaling methodology for aldehyde oxidase substrates to enable selection of appropriate species for traditional allometry. *Xenobiotica***:** Mar 10:1-13. [Epub ahead of print]

Crouch RD, Morrison RD, Byers FW, Lindsley CW, Emmitte KA, and Daniels JS (2016) Evaluating the Disposition of a Mixed Aldehyde Oxidase/Cytochrome P450 Substrate in Rats with Attenuated P450 Activity. *Drug Metab Dispos* **44:**1296-1303.

Dalvie D, Sun H, Xiang C, Hu Q, Jiang Y, and Kang P (2012) Effect of structural variation on aldehyde oxidase-catalyzed oxidation of zoniporide. *Drug Metab Dispos* **40:**1575-1587.

Dalvie D, Xiang C, Kang P, and Zhou S (2013) Interspecies variation in the metabolism of zoniporide by aldehyde oxidase. *Xenobiotica* **43:**399-408.

Decker DE and Levinson DJ (1982) Quantitation of rat liver xanthine oxidase by radioimmunoassay. A mechanism for sex-specific differences. *Arthritis and rheumatism* **25:**326-332.

Diamond S, Boer J, Maduskuie TP, Jr., Falahatpisheh N, Li Y, and Yeleswaram S (2010) Species-specific metabolism of SGX523 by aldehyde oxidase and the toxicological implications. *Drug Metab Dispos* **38:**1277-1285.

Dittrich C, Greim G, Borner M, Weigang-Köhler K, Huisman H, Amelsberg A, Ehret A, Wanders J, Hanauske A, and Fumoleau P (2002) Phase I and pharmacokinetic study of BIBX 1382 BS, an epidermal growth factor receptor (EGFR) inhibitor, given in a continuous daily oral administration. *European Journal of Cancer* **38:**1072-1080.

Felts AS, Rodriguez AL, Blobaum AL, Morrison RD, Bates BS, Thompson Gray A, Rook JM, Tantawy MN, Byers FW, Chang S, Venable DF, Luscombe VB, Tamagnan GD, Niswender CM, Daniels JS, Jones CK, Conn PJ, Lindsley CW, and Emmitte KA (2017) Discovery of N-(5-Fluoropyridin-2-yl)-6-methyl-4-(pyrimidin-5-yloxy)picolinamide (VU0424238): A Novel Negative Allosteric Modulator of Metabotropic Glutamate Receptor Subtype 5 Selected for Clinical Evaluation. *Journal of medicinal chemistry* **60:**5072-5085.

Felts AS, Rodriguez AL, Morrison RD, Venable DF, Manka JT, Bates BS, Blobaum AL, Byers FW, Daniels JS, Niswender CM, Jones CK, Conn PJ, Lindsley CW, and Emmitte KA (2013)

Discovery of VU0409106: A negative allosteric modulator of mGlu5 with activity in a mouse model of anxiety. *Bioorg Med Chem Lett* **23:**5779-5785.

Fu C, Di L, Han X, Soderstrom C, Snyder M, Troutman MD, Obach RS, and Zhang H (2013) Aldehyde oxidase 1 (AOX1) in human liver cytosols: quantitative characterization of AOX1 expression level and activity relationship. *Drug Metab Dispos* **41:**1797-1804.

Fukiya K, Itoh K, Yamaguchi S, Kishiba A, Adachi M, Watanabe N, and Tanaka Y (2010) A single amino acid substitution confers high cinchonidine oxidation activity comparable with that of rabbit to monkey aldehyde oxidase 1. *Drug Metab Dispos* **38:**302-307.

Garattini E and Terao M (2012) The role of aldehyde oxidase in drug metabolism. *Expert Opinion on Drug Metabolism & Toxicology* **8:**487-503.

Hutzler JM, Cerny MA, Yang YS, Asher C, Wong D, Frederick K, and Gilpin K (2014a) Cynomolgus monkey as a surrogate for human aldehyde oxidase metabolism of the EGFR inhibitor BIBX1382. *Drug Metab Dispos* **42:**1751-1760.

Hutzler JM, Yang Y-S, Albaugh D, Fullenwider CL, Schmenk J, and Fisher MB (2012) Characterization of Aldehyde Oxidase Enzyme Activity in Cryopreserved Human Hepatocytes. *Drug Metabolism and Disposition* **40:**267-275.

Hutzler JM, Yang Y-S, Brown C, Heyward S, and Moeller T (2014b) Aldehyde Oxidase Activity in Donor-Matched Fresh and Cryopreserved Human Hepatocytes and Assessment of Variability in 75 Donors. *Drug Metabolism and Disposition* **42:**1090-1097.

Infante JR, Rugg T, Gordon M, Rooney I, Rosen L, Zeh K, Liu R, Burris HA, and Ramanathan RK (2013) Unexpected renal toxicity associated with SGX523, a small molecule inhibitor of MET. *Invest New Drugs* **31:**363-369.

Itoh K, Yamamura M, Takasaki W, Sasaki T, Masubuchi A, and Tanaka Y (2006) Species differences in enantioselective 2-oxidations of RS-8359, a selective and reversible MAO-A inhibitor, and cinchona alkaloids by aldehyde oxidase. *Biopharm Drug Dispos* **27:**133-139.

Jensen KG, Jacobsen AM, Bundgaard C, Nilausen DO, Thale Z, Chandrasena G, and Jorgensen M (2017) Lack of Exposure in a First-in-Man Study Due to Aldehyde Oxidase Metabolism: Investigated by Use of 14C-microdose, Humanized Mice, Monkey Pharmacokinetics, and In Vitro Methods. *Drug Metab Dispos* **45:**68-75.

Johnson C, Stubley-Beedham C, and Stell JG (1985) Hydralazine: a potent inhibitor of aldehyde oxidase activity in vitro and in vivo. *Biochem Pharmacol* **34:**4251-4256.

Jones JP and Korzekwa KR (2013) Predicting intrinsic clearance for drugs and drug candidates metabolized by aldehyde oxidase. *Mol Pharm* **10:**1262-1268.

Kawashima K, Hosoi K, Naruke T, Shiba T, Kitamura M, and Watabe T (1999) Aldehyde oxidase-dependent marked species difference in hepatic metabolism of the sedative-hypnotic, zaleplon, between monkeys and rats. *Drug Metab Dispos* **27:**422-428.

Kitamura S, Sugihara K, Nakatani K, Ohta S, Ohhara T, Ninomiya S, Green CE, and Tyson CA (1999) Variation of hepatic methotrexate 7-hydroxylase activity in animals and humans. *IUBMB Life* **48:**607-611.

Kitamura S, Sugihara K, and Ohta S (2006) Drug-metabolizing ability of molybdenum hydroxylases. *Drug Metab Pharmacokinet* **21:**83-98.

Klecker RW, Cysyk RL, and Collins JM (2006) Zebularine metabolism by aldehyde oxidase in hepatic cytosol from humans, monkeys, dogs, rats, and mice: influence of sex and inhibitors. *Bioorg Med Chem* **14:**62-66.

Kucukgoze G, Terao M, Garattini E, and Leimkuhler S (2017) Direct Comparison of the Enzymatic Characteristics and Superoxide Production of the Four Aldehyde Oxidase Enzymes Present in Mouse. *Drug Metab Dispos* **45:**947-955.

Lepri S, Ceccarelli M, Milani N, Tortorella S, Cucco A, Valeri A, Goracci L, Brink A, and Cruciani G (2017) Structure-metabolism relationships in human-AOX: Chemical insights from a large database of aza-aromatic and amide compounds. *Proc Natl Acad Sci U S A* **114:**E3178-E3187.

Levinson DJ and Chalker D (1980) Rat hepatic xanthine oxidase activity: age and sex specific differences. *Arthritis and rheumatism* **23:**77-82.

Lolkema MP, Bohets HH, Arkenau HT, Lampo A, Barale E, de Jonge MJ, van Doorn L, Hellemans P, de Bono JS, and Eskens FA (2015) The c-Met Tyrosine Kinase Inhibitor JNJ-38877605 Causes Renal Toxicity through Species-Specific Insoluble Metabolite Formation. *Clin Cancer Res* **21:**2297-2304.

Mahro M, Bras NF, Cerqueira NM, Teutloff C, Coelho C, Romao MJ, and Leimkuhler S (2013) Identification of crucial amino acids in mouse aldehyde oxidase 3 that determine substrate specificity. *PloS one* **8:**e82285.

Massey V, Komai H, Palmer G, and Elion GB (1970) On the mechanism of inactivation of xanthine oxidase by allopurinol and other pyrazolo[3,4-d]pyrimidines. *J Biol Chem* **245:**2837-2844.

Morrison RD, Blobaum AL, Byers FW, Santomango TS, Bridges TM, Stec D, Brewer KA, Sanchez-Ponce R, Corlew MM, Rush R, Felts AS, Manka J, Bates BS, Venable DF, Rodriguez AL, Jones CK, Niswender CM, Conn PJ, Lindsley CW, Emmitte KA, and Daniels JS (2012) The Role of Aldehyde Oxidase and Xanthine Oxidase in the Biotransformation of a Novel Negative Allosteric Modulator of Metabotropic Glutamate Receptor Subtype 5. *Drug Metabolism and Disposition* **40:**1834-1845.

Pritsos CA (2000) Cellular distribution, metabolism and regulation of the xanthine oxidoreductase enzyme system. *Chemico-biological interactions* **129:**195-208.

Pryde DC, Dalvie D, Hu Q, Jones P, Obach RS, and Tran T-D (2010) Aldehyde Oxidase: An Enzyme of Emerging Importance in Drug Discovery. *Journal of medicinal chemistry* **53:**8441-8460.

Rashidi MR, Smith JA, Clarke SE, and Beedham C (1997) In vitro oxidation of famciclovir and 6-deoxypenciclovir by aldehyde oxidase from human, guinea pig, rabbit, and rat liver. *Drug Metab Dispos* **25:**805-813.

Sharma R, Eng H, Walker GS, Barreiro G, Stepan AF, McClure KF, Wolford A, Bonin PD, Cornelius P, and Kalgutkar AS (2011) Oxidative metabolism of a quinoxaline derivative by xanthine oxidase in rodent plasma. *Chem Res Toxicol* **24:**2207-2216.

Smeland E, Fuskevag OM, Nymann K, Svendesn JS, Olsen R, Lindal S, Bremnes RM, and Aarbakke J (1996) High-dose 7-hydromethotrexate: acute toxicity and lethality in a rat model. *Cancer Chemother Pharmacol* **37:**415-422.

Strelevitz TJ, Orozco CC, and Obach RS (2012) Hydralazine As a Selective Probe Inactivator of Aldehyde Oxidase in Human Hepatocytes: Estimation of the Contribution of Aldehyde Oxidase to Metabolic Clearance. *Drug Metabolism and Disposition* **40:**1441-1448.

Terao M, Romao MJ, Leimkuhler S, Bolis M, Fratelli M, Coelho C, Santos-Silva T, and Garattini E (2016) Structure and function of mammalian aldehyde oxidases. *Arch Toxicol* **90:**753-780.

Vila R, Kurosaki M, Barzago MM, Kolek M, Bastone A, Colombo L, Salmona M, Terao M, and Garattini E (2004) Regulation and biochemistry of mouse molybdo-flavoenzymes. The DBA/2 mouse is selectively deficient in the expression of aldehyde oxidase homologues 1 and 2 and represents a unique source for the purification and characterization of aldehyde oxidase. *J Biol Chem* **279:**8668-8683.

Xu Y, Li L, Wang Y, Xing J, Zhou L, Zhong D, Luo X, Jiang H, Chen K, Zheng M, Deng P, and Chen X (2017) Aldehyde Oxidase Mediated Metabolism in Drug-like Molecules: A Combined Computational and Experimental Study. *Journal of medicinal chemistry* **60:**2973-2982.

Zientek MA and Youdim K (2015) Reaction phenotyping: advances in the experimental strategies used to characterize the contribution of drug-metabolizing enzymes. *Drug Metab Dispos* **43:**163-181.

Footnotes

The authors gratefully acknowledge financial support from the Warren Family and Foundation and establishment of the William K. Warren, Jr. Chair in Medicine (CWL).

Figure Legends

Figure 1. Proposed metabolism of VU238 to major metabolites M1 and M2 in hepatic S9 (absent NADPH) of human, monkey, rat, mouse, guinea pig, and minipig. M2 was not detected in extracts from incubations of VU238 with human and minipig S9, but was only detected in extracts from direct incubations with M1 (VU922).

Figure 2. LC/MS/MS spectra of **(A)** VU238, and metabolites **(B)** M1 (VU922) and **(C)** M2 obtained from either synthetic standard solutions (A and B) or extract from male cynomolgus monkey hepatic S9 incubation with VU238 (C).

Figure 3. LC-UV chromatograms and mass spectra of VU238, VU180, M1 and, M2 obtained from extracts of incubations with VU238 or VU180 (20 μM) in male cynomolgus monkey hepatic S9 (5 mg/mL). **(A)** LC-UV chromatograms obtained from extracts of incubations with VU238 (top) or VU180 (bottom). **(B)** Mass spectra of VU238 (top) or VU180 (bottom). **(C)** Mass spectra of M1 obtained from extracts of incubations with VU238 (top) or VU180 (bottom). **(D)** Mass spectra of M2 obtained from extracts of incubations with VU238 (top) or VU180 (bottom).

Figure 4. Extracted ion chromatograms (XIC) obtained from extracts of incubations with VU238 (5 μM) in **(A)** male cynomolgus monkey hepatic S9 (2 mg/mL) and **(B)** male rat hepatic S9 (2 mg/mL) demonstrating formation of M1 and M2 in the presence or absence of the XO inhibitor allopurinol (100 μM) or the AO inhibitor hydralazine (50 μM).

Figure 5. Extracted ion chromatograms (XIC) obtained from extracts of incubations with M1 (VU922, 5 μM) in **(A)** male cynomolgus monkey hepatic S9 (2 mg/mL) and **(B)** male rat hepatic

S9 (2 mg/mL) demonstrating formation of M2 in the presence or absence of the XO inhibitor allopurinol (100 μM) or the AO inhibitor hydralazine (50 μM).

Figure 6. Extracted ion chromatograms (XIC) obtained from extracts of incubations with **(A)** VU238 (5 μM) and **(B)** M1 (VU922, 5 μM) in multiple species' hepatic S9 (2 mg/mL). Human data obtained using mixed gender S9. All other data obtained using male S9.

Figure 7. Extracted ion chromatograms (XIC) obtained from extracts of incubations with VU238 (5 μM) in **(A)** female cynomolgus monkey hepatic S9 (2 mg/mL) and **(B)** female rat hepatic S9 (2 mg/mL) demonstrating formation of M1 and M2 in the presence or absence of the XO inhibitor allopurinol (100 μM) or the AO inhibitor hydralazine (50 μM).

Figure 8. Extracted ion chromatograms (XIC) obtained from extracts of incubations with M1 (VU922, 5 μM) in **(A)** female cynomolgus monkey hepatic S9 (2 mg/mL) and **(B)** female rat hepatic S9 (2 mg/mL) demonstrating formation of M2 in the presence or absence of the XO inhibitor allopurinol (100 μM) or the AO inhibitor hydralazine (50 μM).

Figure 9. Extracted ion chromatograms (XIC) obtained from extracts of incubations with BIBX1382 (5 μM) in **(A)** male cynomolgus monkey hepatic S9 (2 mg/mL) and **(B)** male rat hepatic S9 (2 mg/mL) demonstrating formation of M1b and M2b in the presence or absence of the XO inhibitor allopurinol (100 μM) or the AO inhibitor hydralazine (50 μM). **(C)** Summary of BIBX1382 hepatic S9 metabolism in human, monkey, rat, mouse, guinea pig, and minipig. Formation of M1b and M2b in incubations of BIBX1382 with hepatic S9 was inhibited by hydralazine in all species. H, human; C, cynomolgus monkey; Rh, rhesus monkey; R, rat; M, mouse; G, guinea pig; MP, minipig

DMD Fast Forward. Published on September 22, 2017 as DOI: 10.1124/dmd.117.077552
This article has not been copyedited and formatted. The final version may differ from this version.

Tables

Table 1. Proposed predominant metabolic pathway mediating formation of M1 or M2 in multispecies' hepatic S9 (2 mg/mL), determined from incubations of VU238 (5 μM) or M1 (VU922, 5 μM) with the AO inhibitor hydralazine (50 μM) or the XO inhibitor allopurinol (100 μM). Designations of "AO" or "XO" indicate formation of the metabolite was predominantly inhibited by either hydralazine or allopurinol, respectively.

	M1	M2
Human[a]	AO	n.d.
Cynomolgus	AO	AO
Rhesus	AO	AO
Rat	AO	XO
Mouse	AO	XO
Guinea Pig	AO	AO
Minipig	AO	n.d.
Female Cynomolgus	AO	n.d.
Female Rat	AO	XO

[a] Human data obtained using mixed gender S9. All other data obtained using male S9 unless otherwise indicated.

n.d. = not determined

DMD Fast Forward. Published on September 22, 2017 as DOI: 10.1124/dmd.117.077552
This article has not been copyedited and formatted. The final version may differ from this version.

Table 2. Intrinsic clearance (CL_{int}, μL/min/mg protein) obtained from incubations of VU238 (1 μM) or M1 (VU922, 1 μM) with hepatic S9 (2.5 mg/mL) of multiple species.

Species	VU238	VU922 (M1)
Human	1.48 ± 0.312	n.d.
Cynomolgus	12.1 ± 0.643	2.00 ± 0.040
Rhesus	5.15 ± 0.537	1.44 ± 0.139
Rat	13.7 ± 0.265	2.19 ± 0.201
Mouse	4.76 ± 0.386	n.d.
Guinea Pig	1.89 ± 0.180	3.40 ± 0.069
Minipig	3.51 ± 0.306	n.d.

Data represent means ± SD of triplicate determinations.

n.d. = not determined due to low substrate turnover

DMD Fast Forward. Published on September 22, 2017 as DOI: 10.1124/dmd.117.077552
This article has not been copyedited and formatted. The final version may differ from this version.

Figures

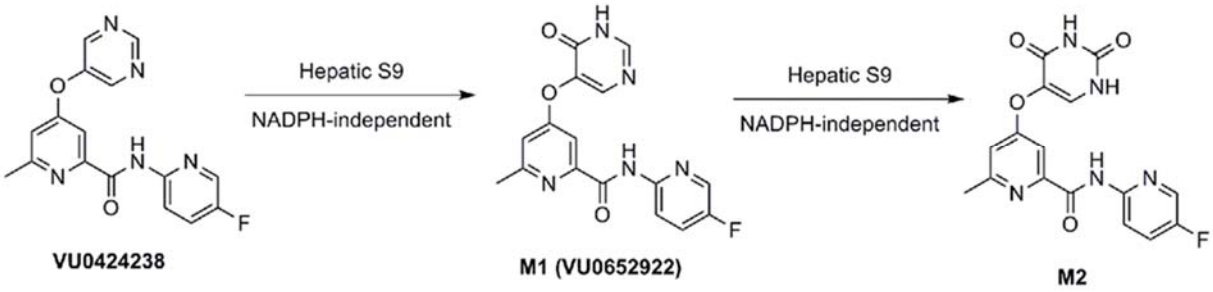

Figure 1

DMD Fast Forward. Published on September 22, 2017 as DOI: 10.1124/dmd.117.077552
This article has not been copyedited and formatted. The final version may differ from this version.

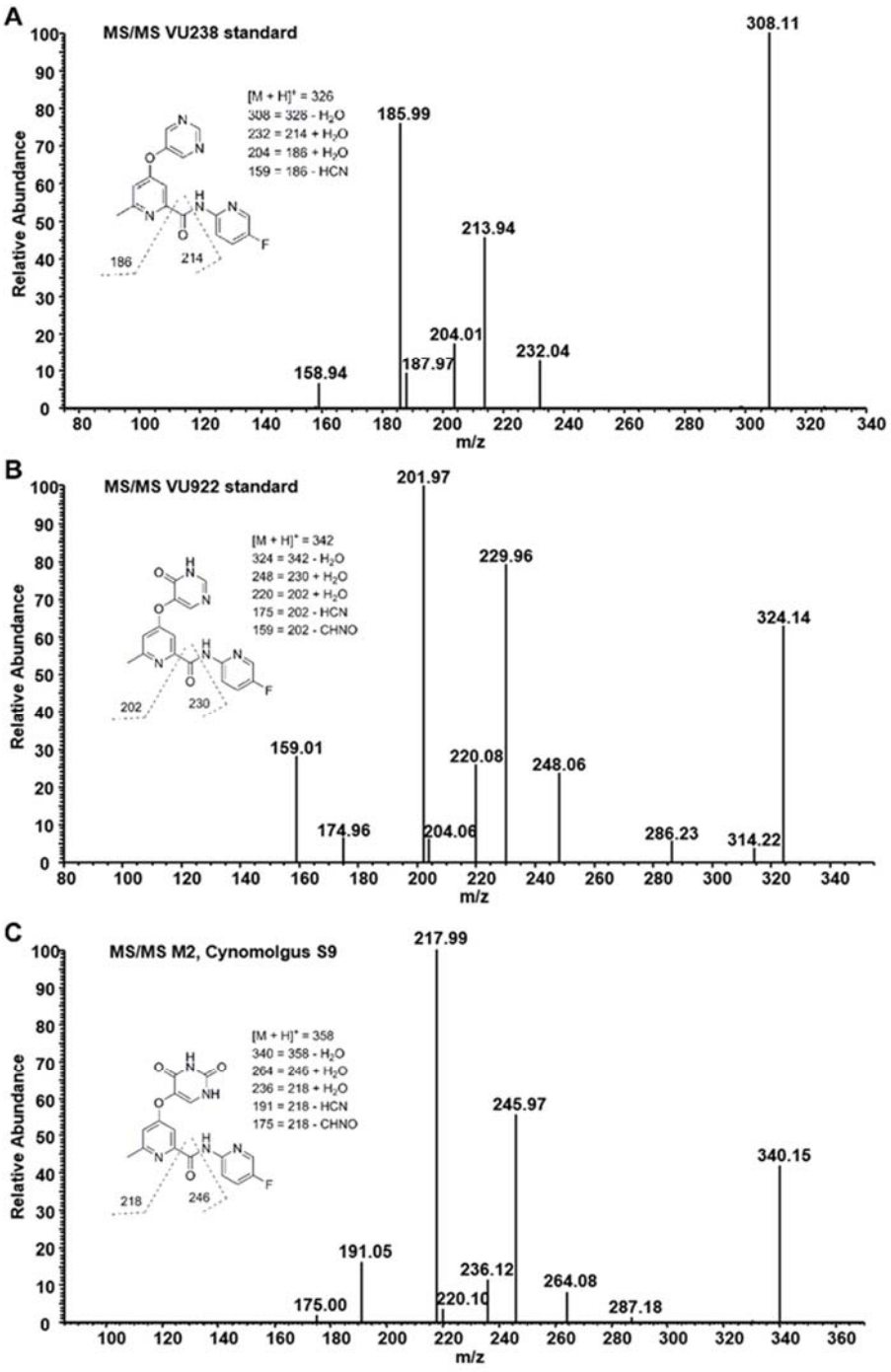

Figure 2

DMD Fast Forward. Published on September 22, 2017 as DOI: 10.1124/dmd.117.077552
This article has not been copyedited and formatted. The final version may differ from this version.

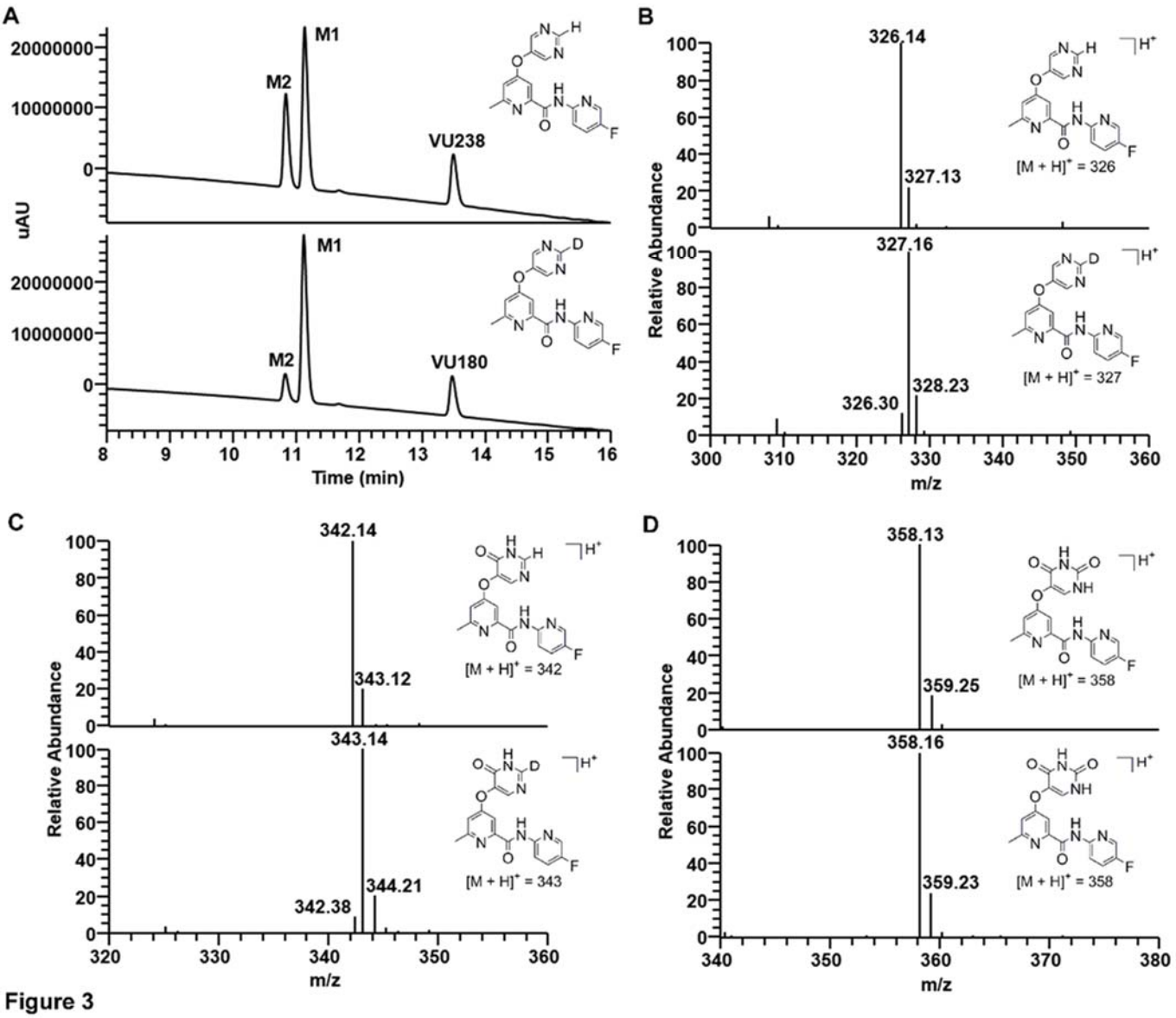

Figure 3

DMD Fast Forward. Published on September 22, 2017 as DOI: 10.1124/dmd.117.077552
This article has not been copyedited and formatted. The final version may differ from this version.

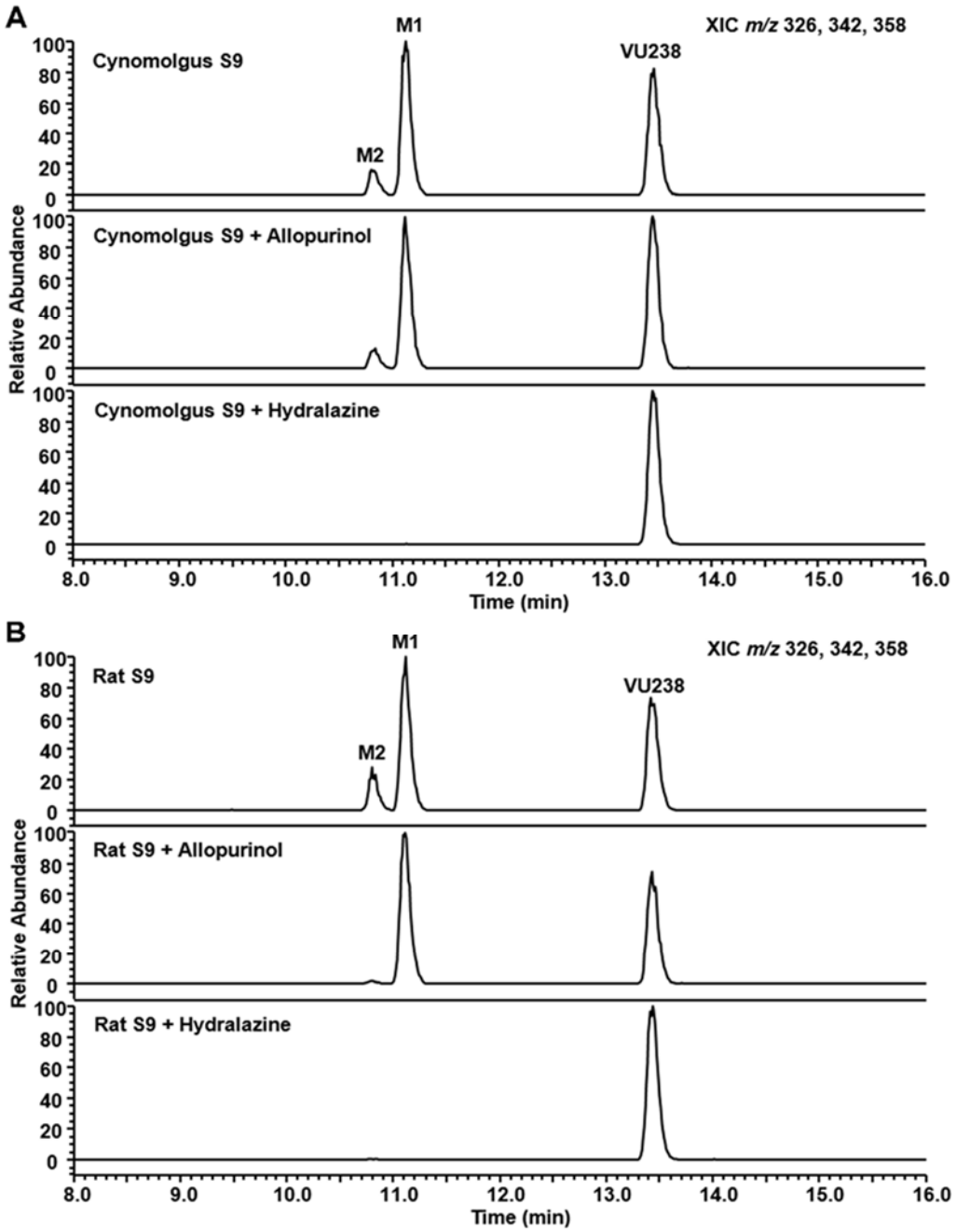

Figure 4

DMD Fast Forward. Published on September 22, 2017 as DOI: 10.1124/dmd.117.077552
This article has not been copyedited and formatted. The final version may differ from this version.

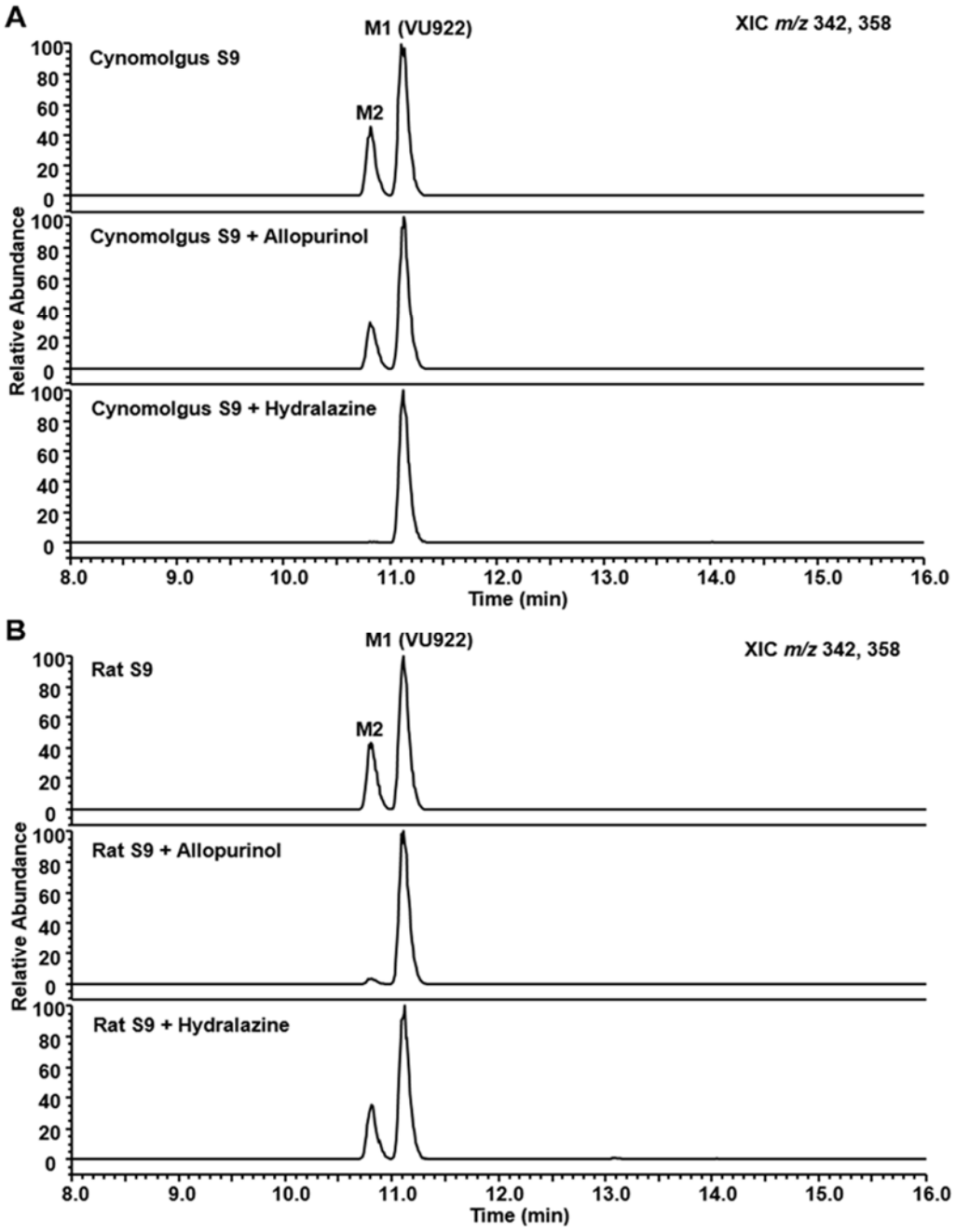

Figure 5

DMD Fast Forward. Published on September 22, 2017 as DOI: 10.1124/dmd.117.077552
This article has not been copyedited and formatted. The final version may differ from this version.

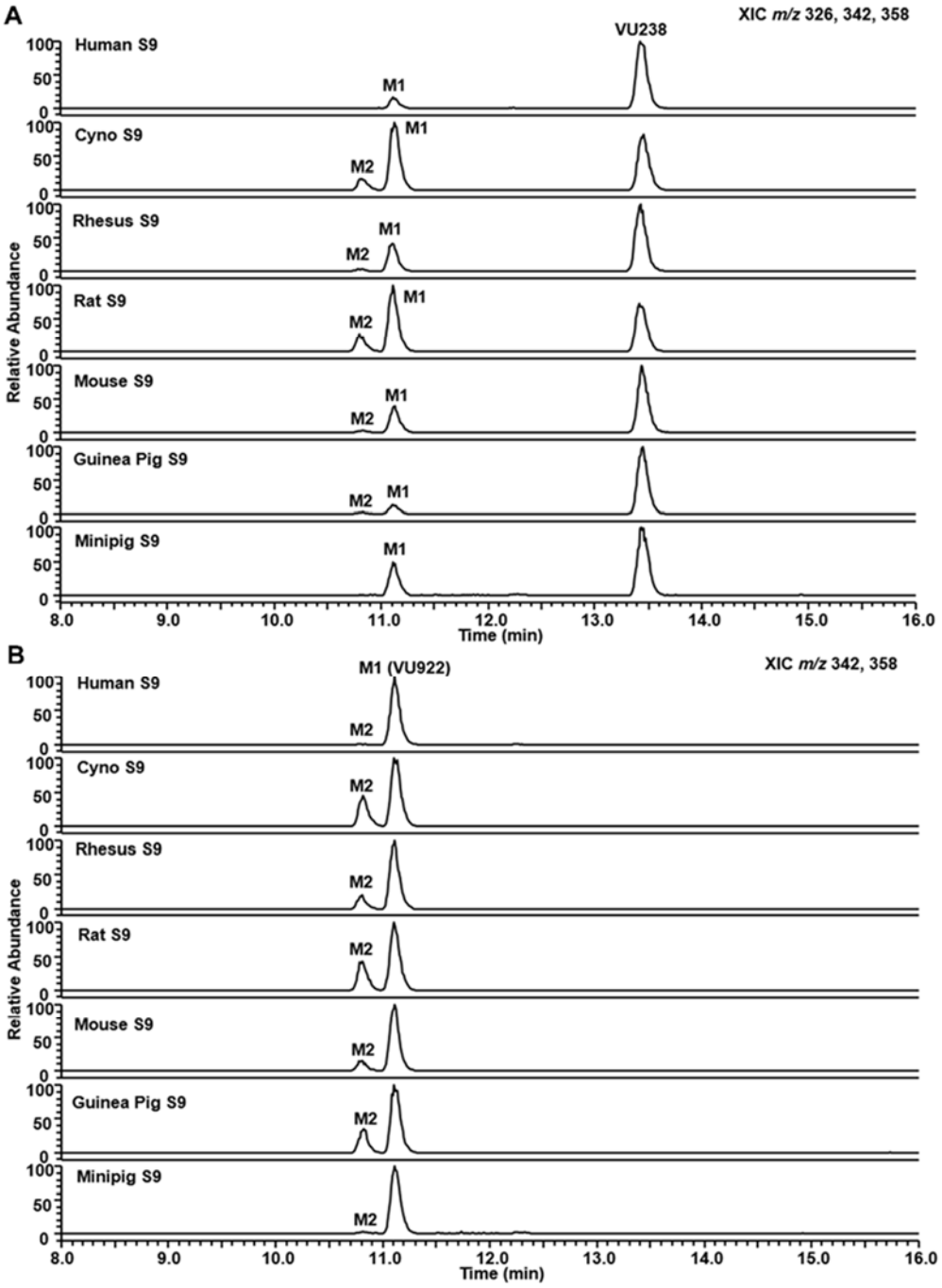

Figure 6

DMD Fast Forward. Published on September 22, 2017 as DOI: 10.1124/dmd.117.077552
This article has not been copyedited and formatted. The final version may differ from this version.

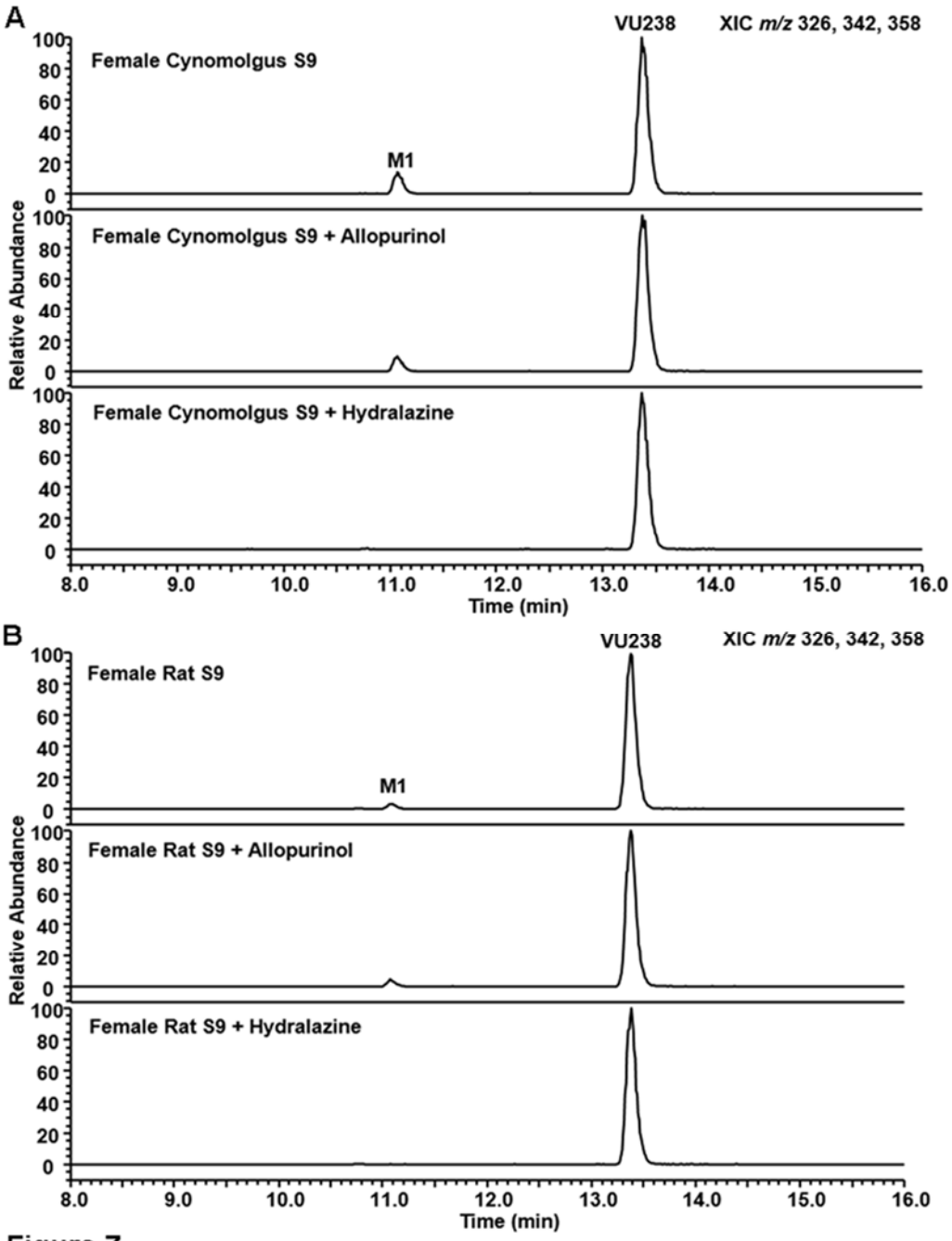

Figure 7

DMD Fast Forward. Published on September 22, 2017 as DOI: 10.1124/dmd.117.077552
This article has not been copyedited and formatted. The final version may differ from this version.

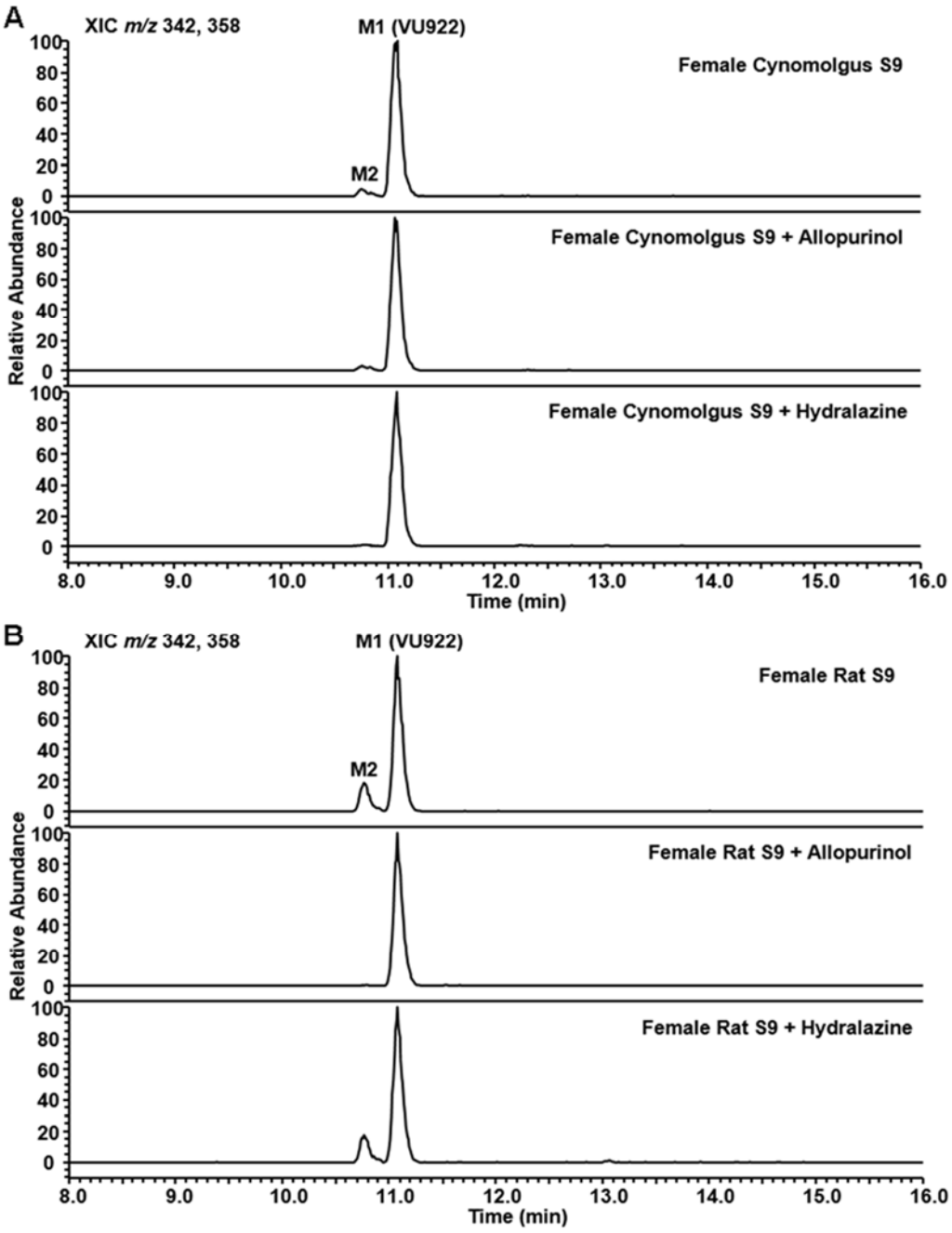

Figure 8

DMD Fast Forward. Published on September 22, 2017 as DOI: 10.1124/dmd.117.077552
This article has not been copyedited and formatted. The final version may differ from this version.

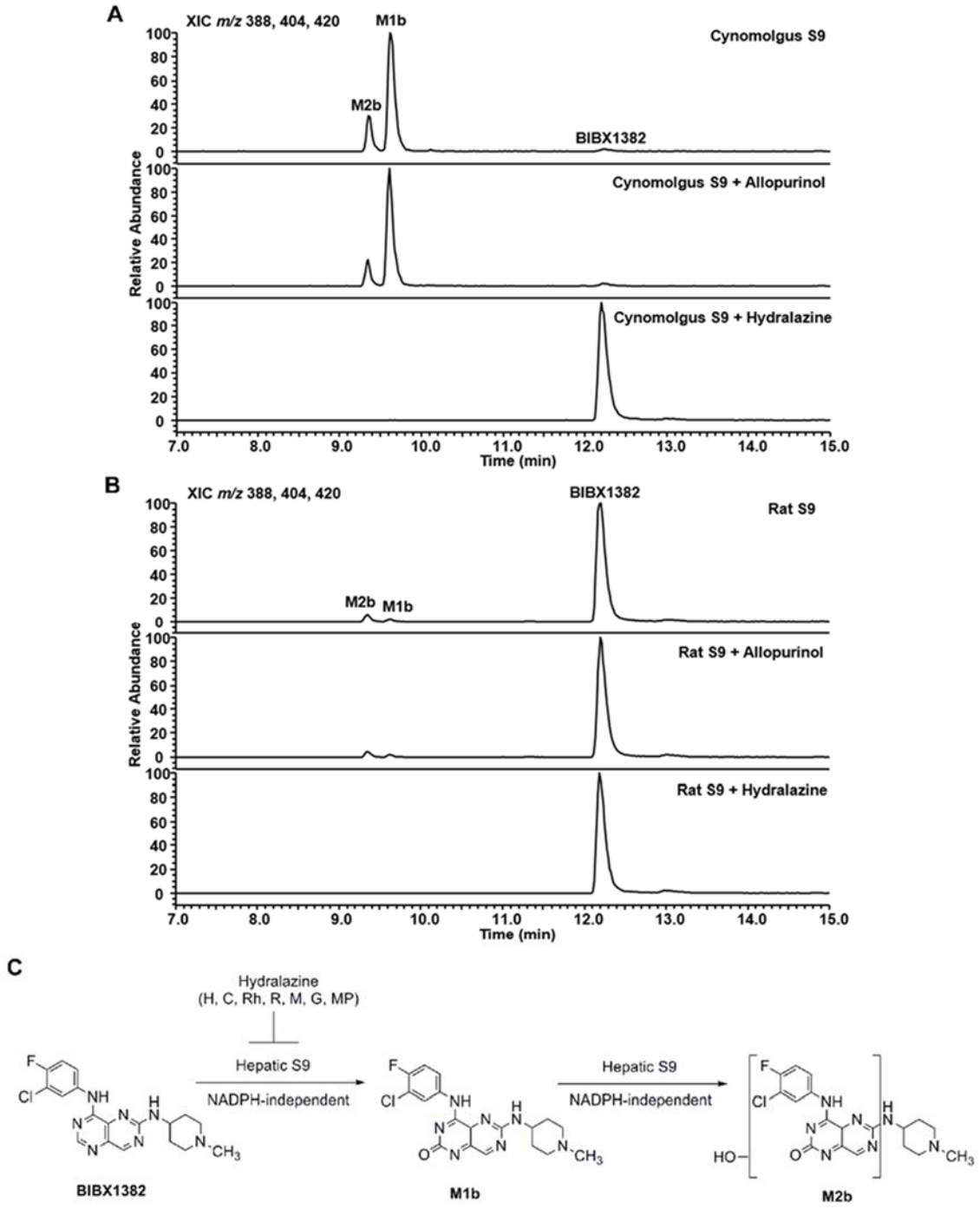

Figure 9

Species-specific involvement of aldehyde oxidase and xanthine oxidase in the metabolism of the pyrimidine-containing $mGlu_5$ negative allosteric modulator VU0424238 (auglurant)

Rachel D. Crouch, Annie L. Blobaum, Andrew S. Felts, P. Jeffrey Conn and Craig W. Lindsley

Drug Metabolism and Disposition

Supplemental Information

Supplemental Figure 1.

Proton NMR spectra for VU0652922 (M1). NMR spectra were recorded on a 400 MHz AMX Bruker NMR spectrometer.

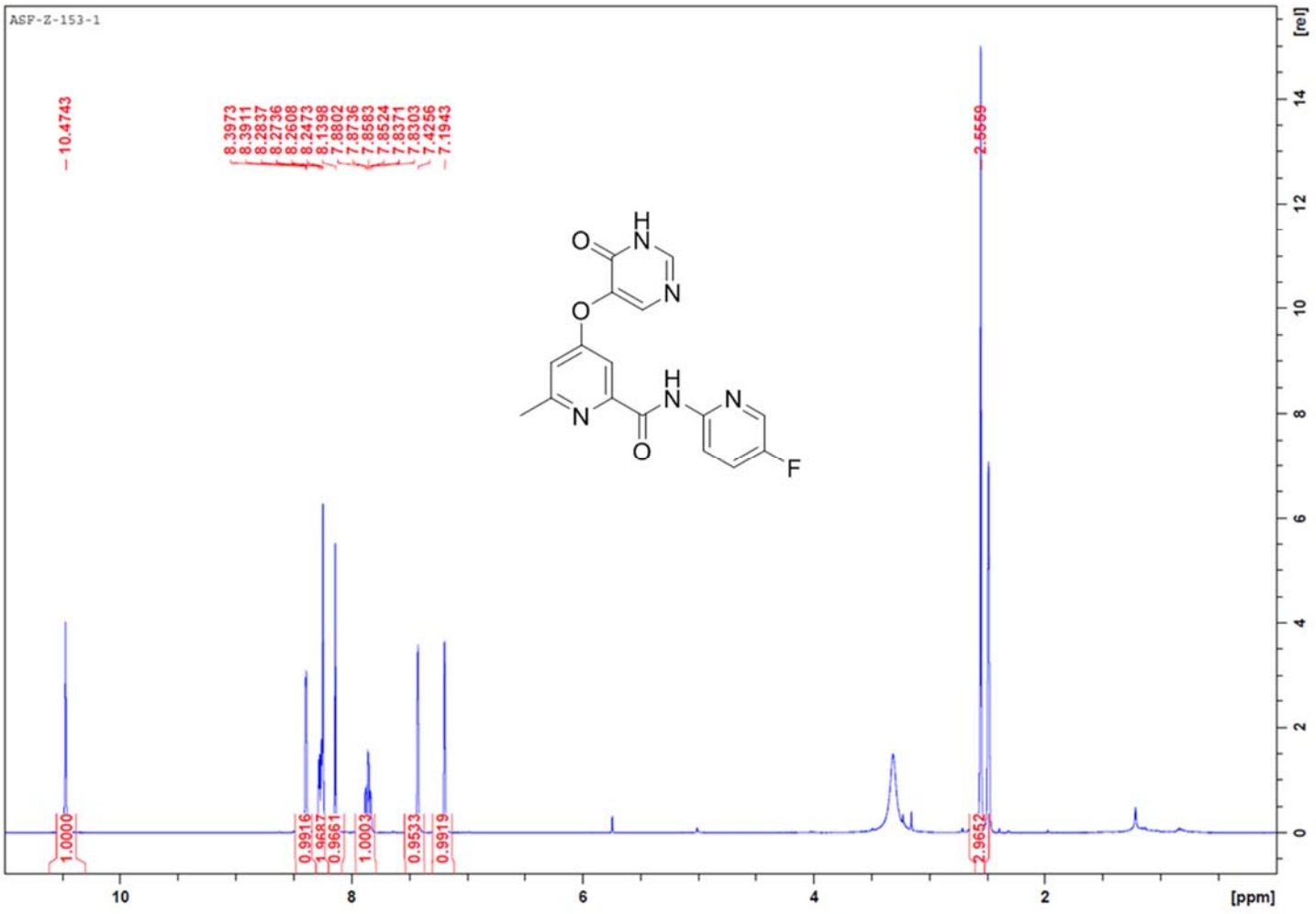

Supplemental Figure 2.

Extracted ion chromatograms (XIC) obtained from extracts of incubations with VU238 (5 μM) in (A) mixed gender human hepatic S9 (2 mg/mL), (B) male rhesus monkey hepatic S9 (2 mg/mL), (C) male mouse hepatic S9 (2 mg/mL), (D) male guinea pig hepatic S9 (2 mg/mL), and (E) male minipig hepatic S9 (2mg/mL) demonstrating formation of M1 and M2 in the presence or absence of the XO inhibitor allopurinol (100 μM) or the AO inhibitor hydralazine (50 μM).

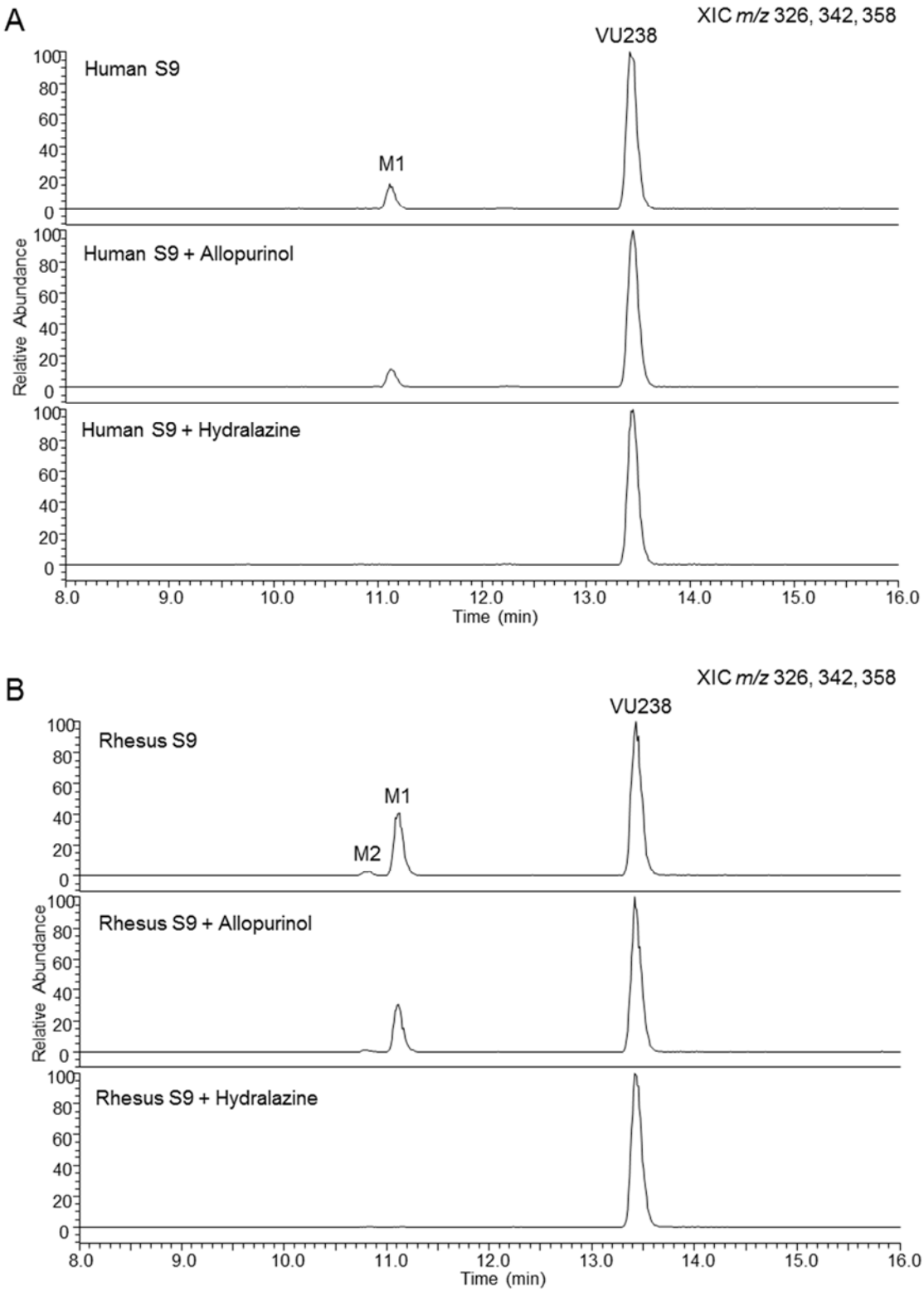

C

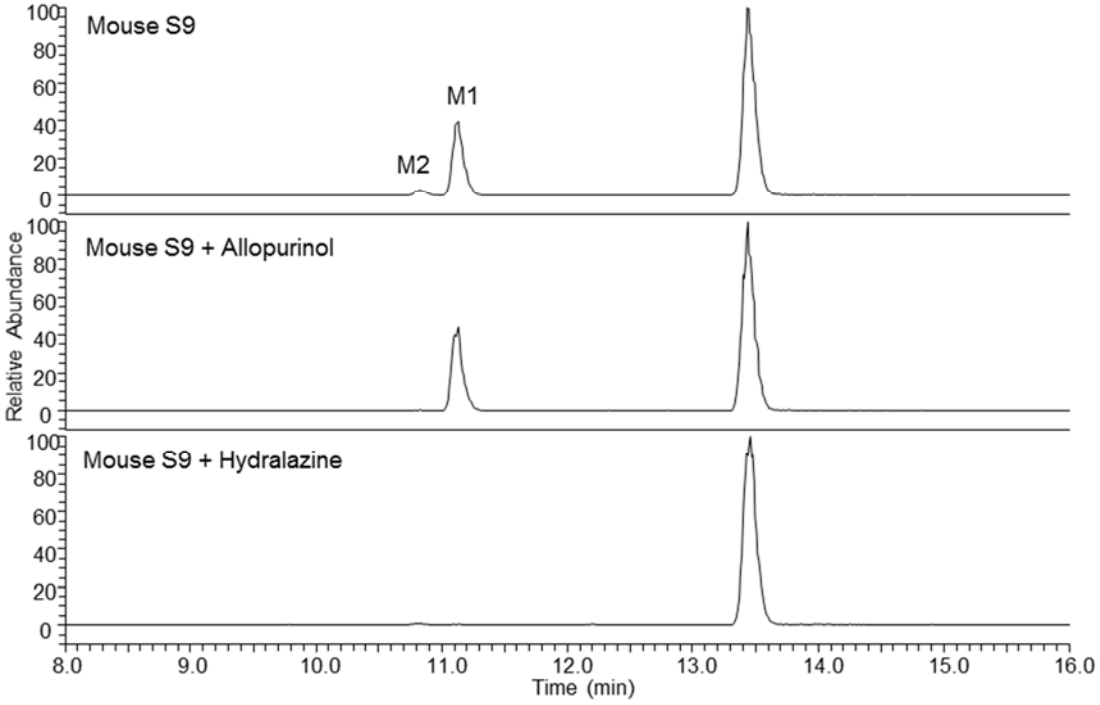
XIC m/z 326, 342, 358
VU238
Mouse S9
M1
M2
Mouse S9 + Allopurinol
Mouse S9 + Hydralazine
Relative Abundance
Time (min)

D

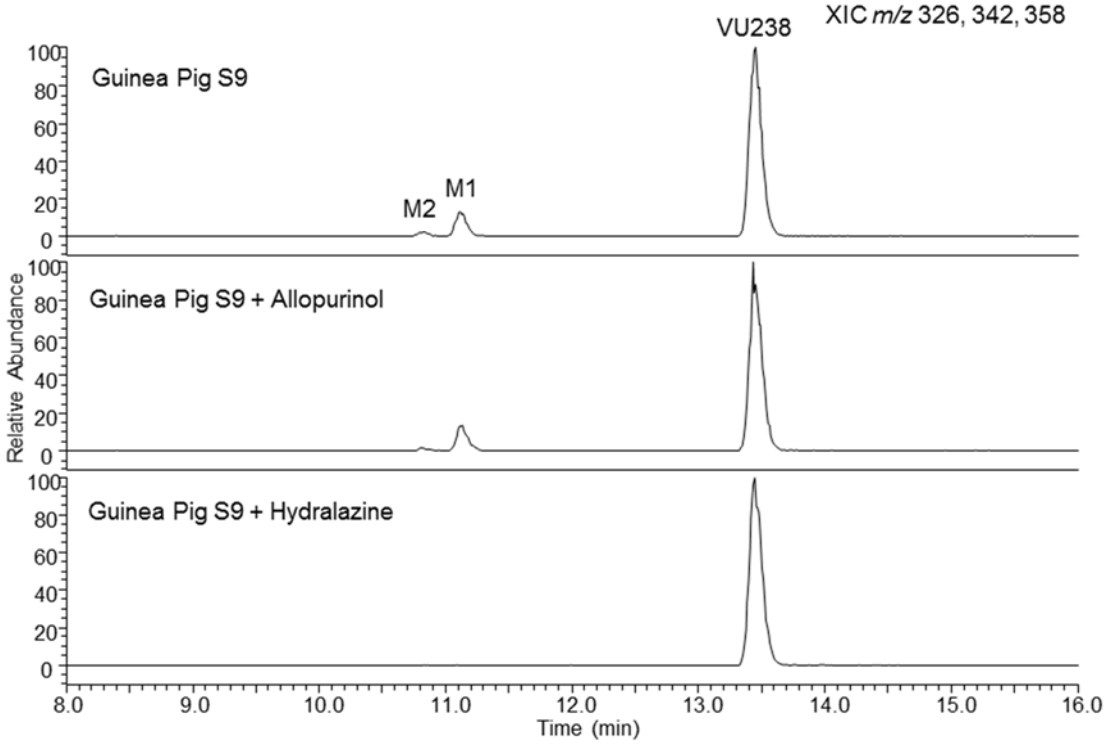
XIC m/z 326, 342, 358
VU238
Guinea Pig S9
M2
M1
Guinea Pig S9 + Allopurinol
Guinea Pig S9 + Hydralazine
Relative Abundance
Time (min)

E

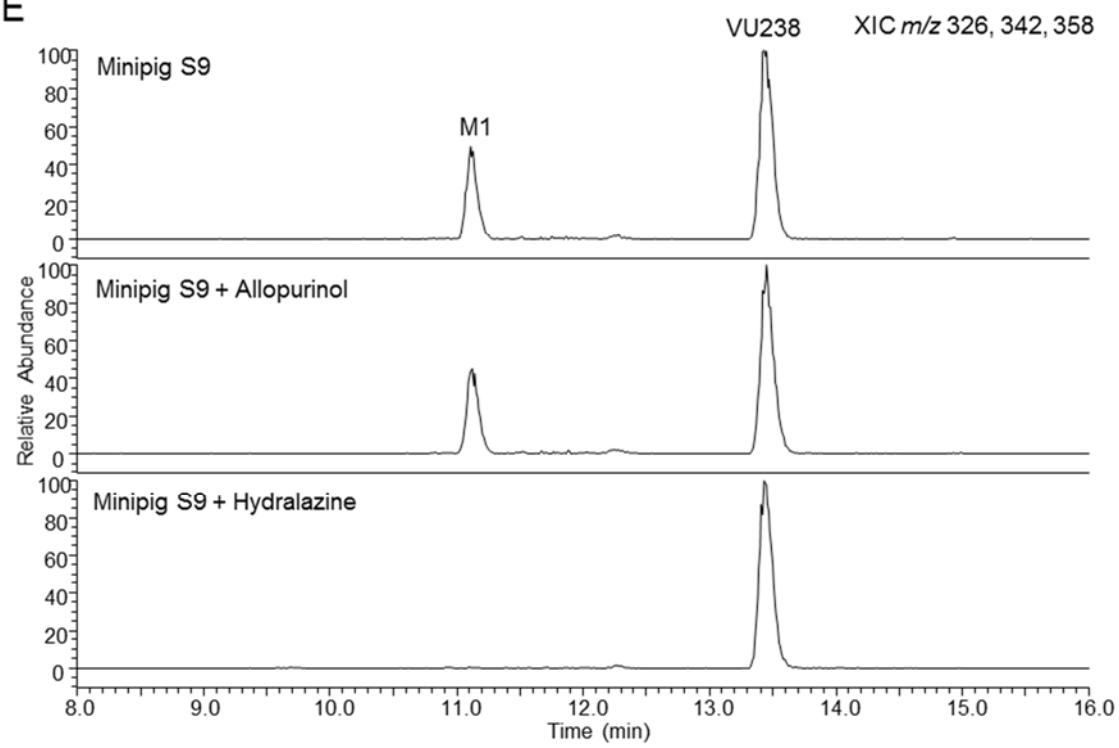
VU238
XIC m/z 326, 342, 358
Minipig S9
M1
Minipig S9 + Allopurinol
Minipig S9 + Hydralazine
Relative Abundance
Time (min)
100
80
60
40
20
0
8.0
9.0
10.0
11.0
12.0
13.0
14.0
15.0
16.0

Supplemental Figure 3.

Extracted ion chromatograms (XIC) obtained from extracts of incubations with VU922 (5 μM) in (A) mixed gender human hepatic S9 (2 mg/mL), (B) male rhesus monkey hepatic S9 (2 mg/mL), (C) male mouse hepatic S9 (2 mg/mL), (D) male guinea pig hepatic S9 (2 mg/mL), and (E) male minipig hepatic S9 (2mg/mL) demonstrating formation of M2 in the presence or absence of the XO inhibitor allopurinol (100 μM) or the AO inhibitor hydralazine (50 μM).

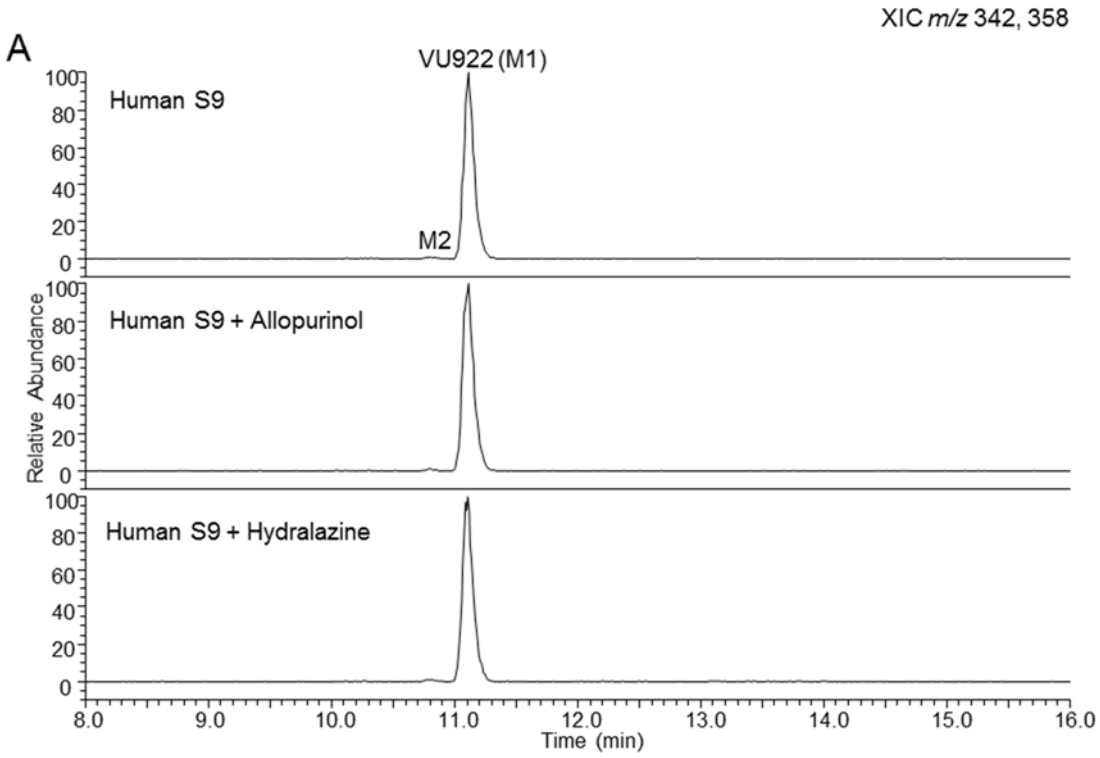

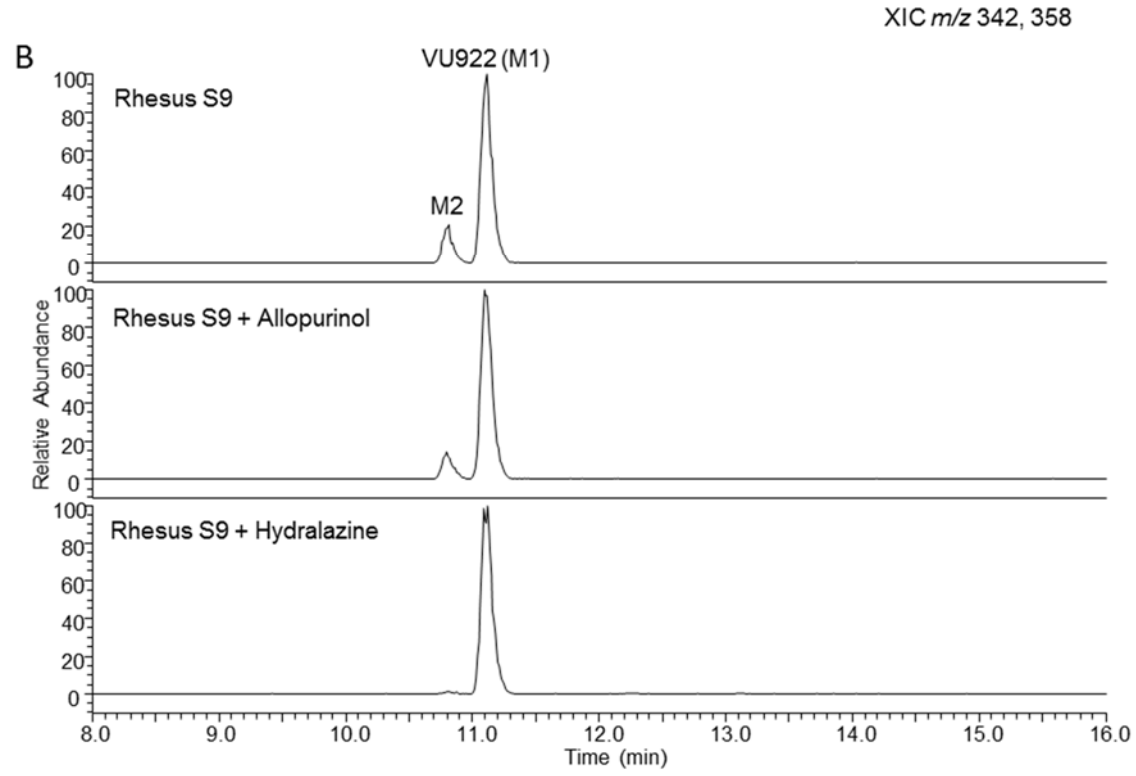
XIC m/z 342, 358
B
VU922 (M1)
M2
Rhesus S9
Rhesus S9 + Allopurinol
Rhesus S9 + Hydralazine
Relative Abundance
Time (min)

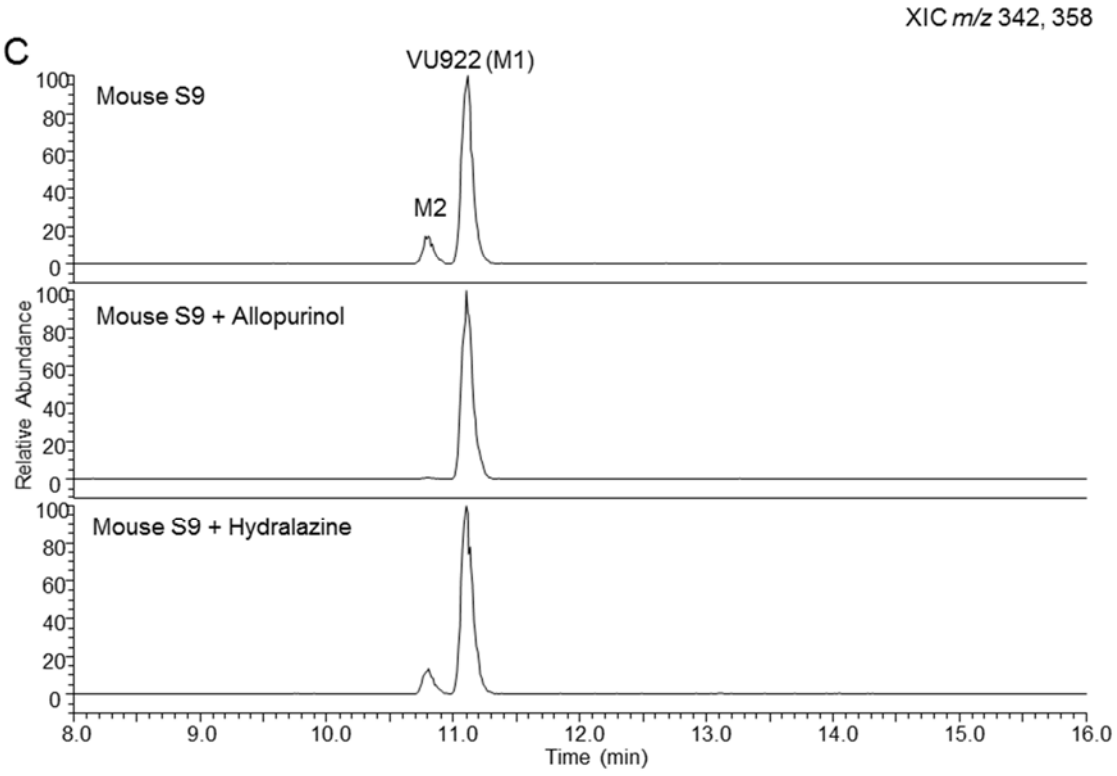
XIC m/z 342, 358
C
VU922 (M1)
M2
Mouse S9
Mouse S9 + Allopurinol
Mouse S9 + Hydralazine
Relative Abundance
Time (min)

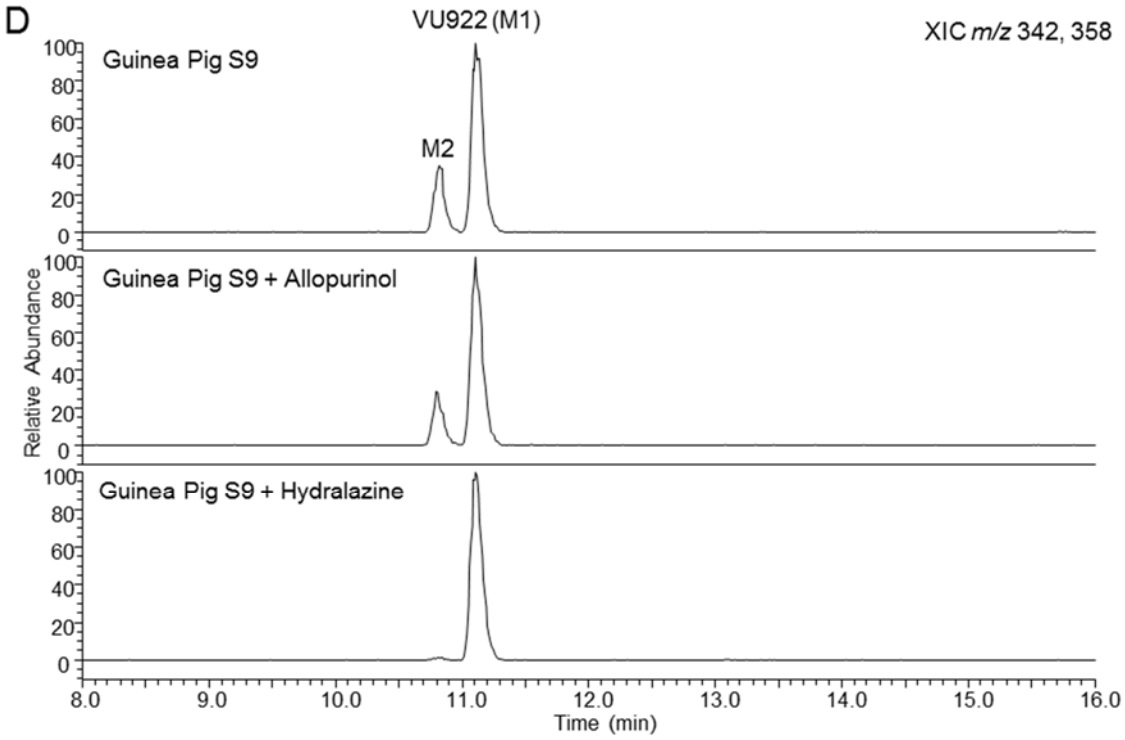
D
VU922 (M1)
XIC m/z 342, 358
Guinea Pig S9
M2
Guinea Pig S9 + Allopurinol
Guinea Pig S9 + Hydralazine
Relative Abundance
Time (min)

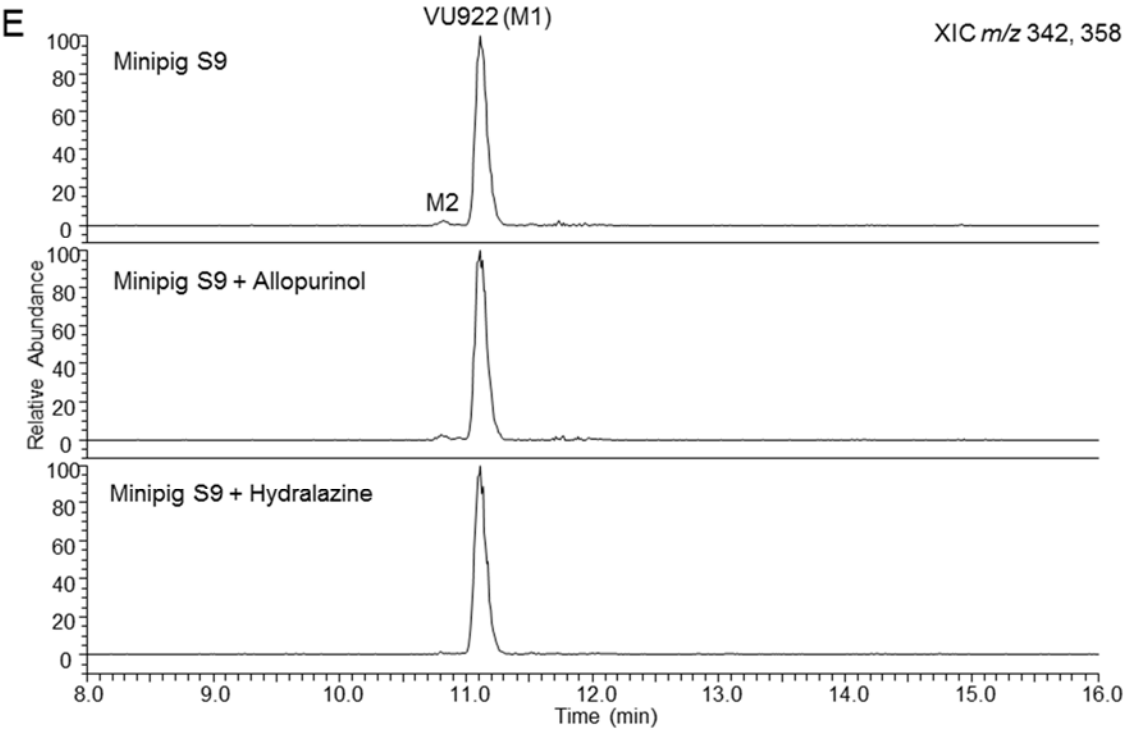
E
VU922 (M1)
XIC m/z 342, 358
Minipig S9
M2
Minipig S9 + Allopurinol
Minipig S9 + Hydralazine
Relative Abundance
Time (min)

Supplemental Figure 4.

Extracted ion chromatograms (XIC) obtained from extracts of incubations with BIBX1382 (5 μM) in (A) mixed gender human hepatic S9 (2 mg/mL), (B) male rhesus monkey hepatic S9 (2 mg/mL), (C) male mouse hepatic S9 (2 mg/mL), (D) male guinea pig hepatic S9 (2 mg/mL), and (E) male minipig hepatic S9 (2mg/mL) demonstrating formation of M1b and M2b in the presence or absence of the XO inhibitor allopurinol (100 μM) or the AO inhibitor hydralazine (50 μM).

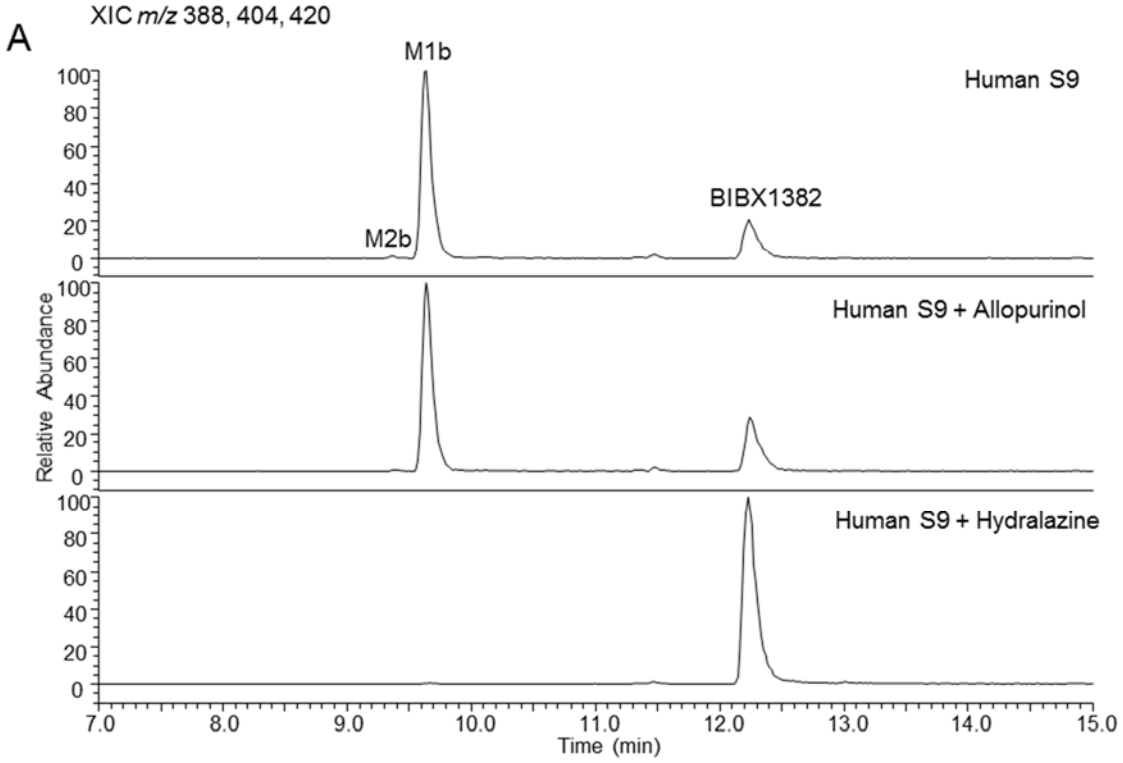

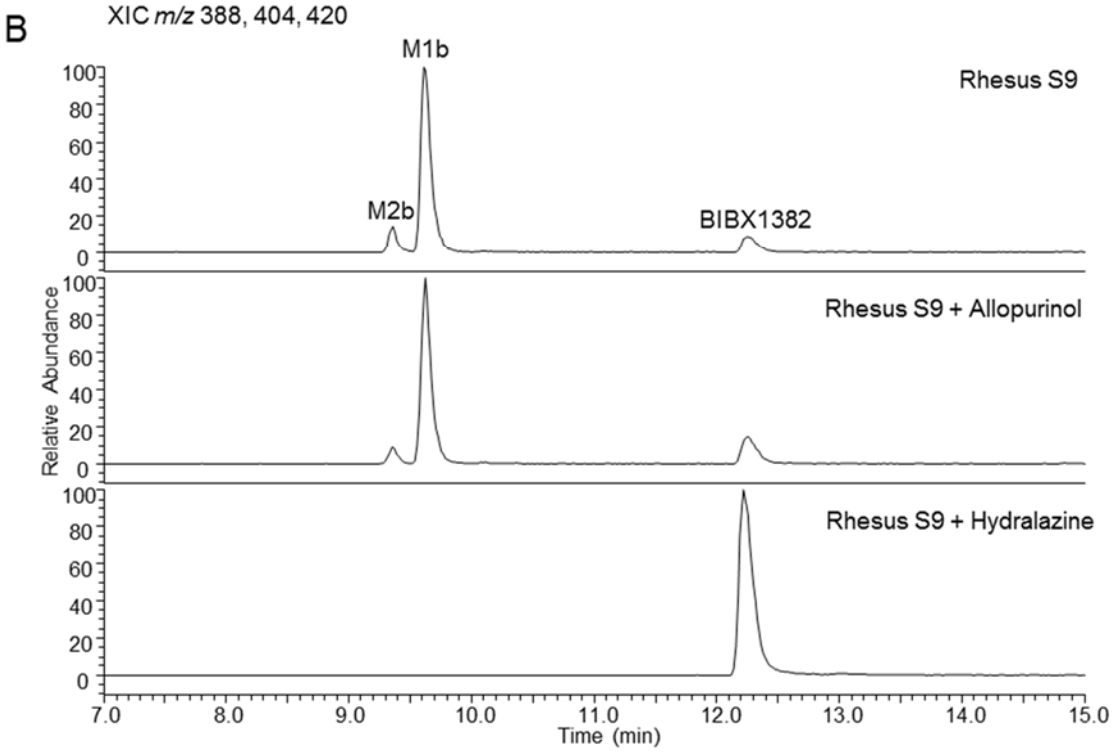
B
XIC m/z 388, 404, 420
M1b
M2b
BIBX1382
Rhesus S9
Rhesus S9 + Allopurinol
Rhesus S9 + Hydralazine
Relative Abundance
Time (min)

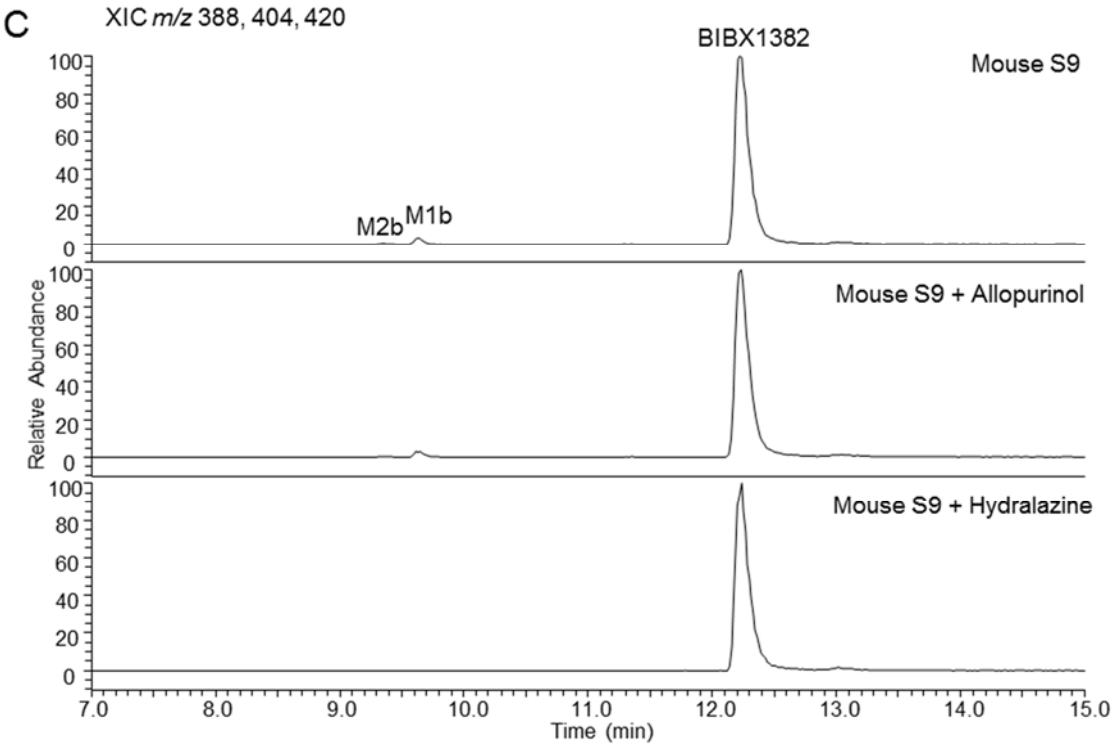
C
XIC m/z 388, 404, 420
BIBX1382
M2b
M1b
Mouse S9
Mouse S9 + Allopurinol
Mouse S9 + Hydralazine
Relative Abundance
Time (min)

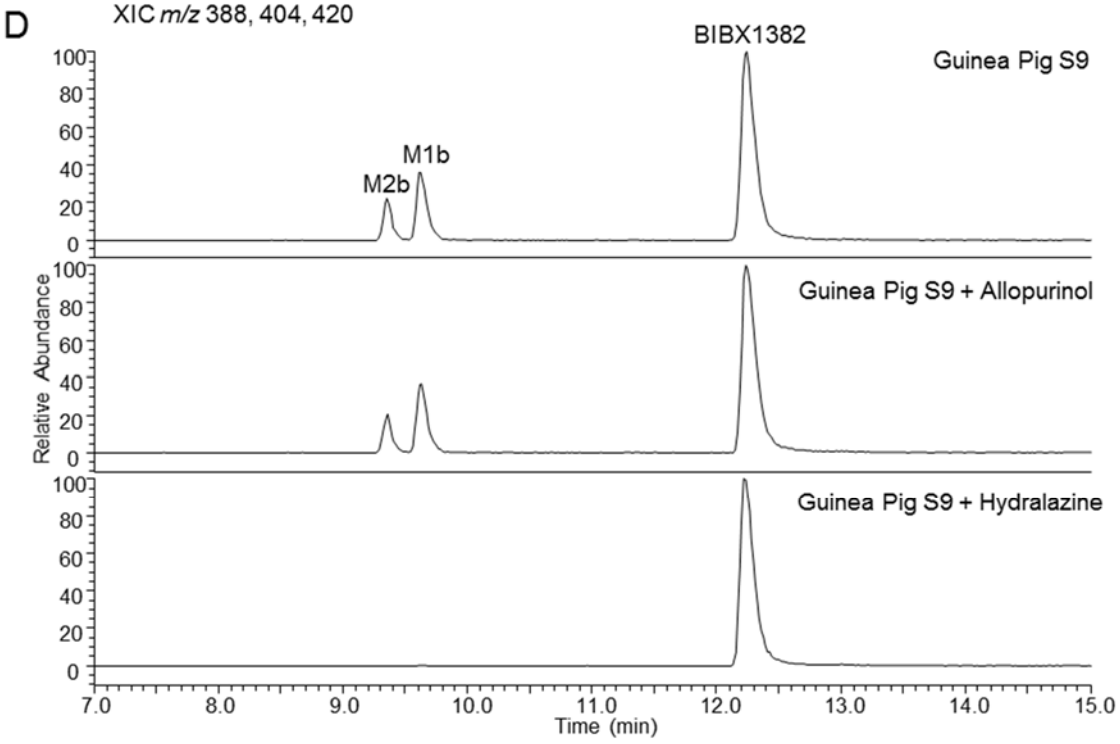
D
XIC m/z 388, 404, 420
BIBX1382
Guinea Pig S9
M1b
M2b
Guinea Pig S9 + Allopurinol
Guinea Pig S9 + Hydralazine
Relative Abundance
Time (min)

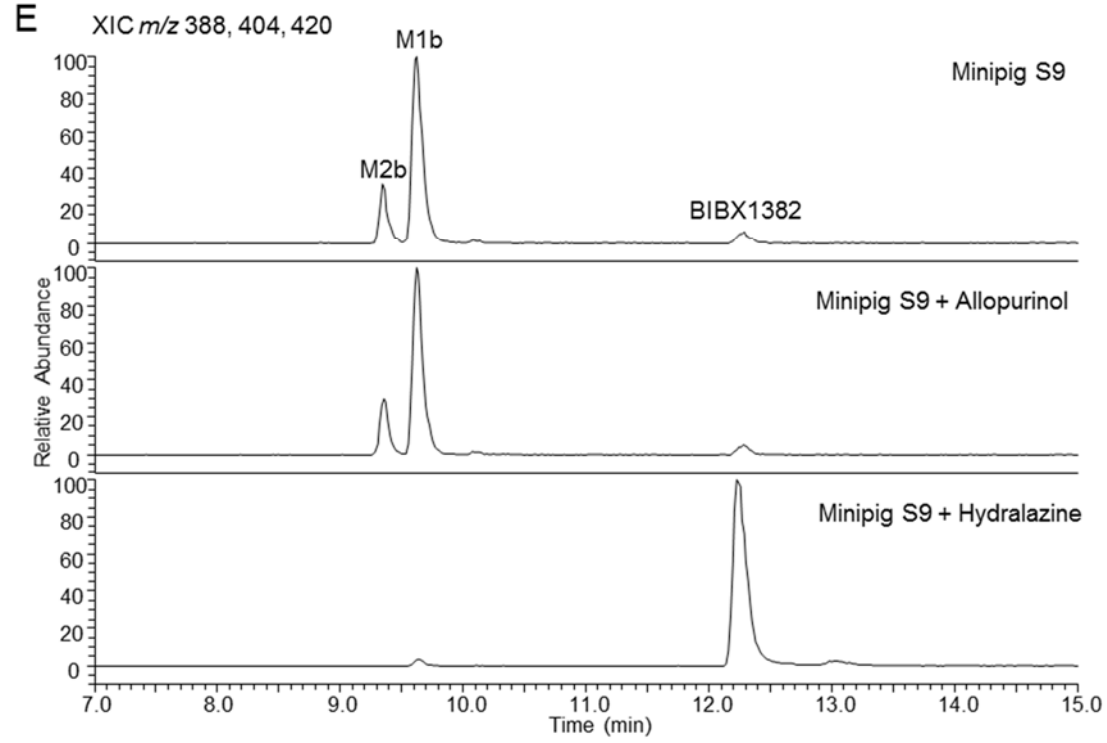
E
XIC m/z 388, 404, 420
M1b
Minipig S9
M2b
BIBX1382
Minipig S9 + Allopurinol
Minipig S9 + Hydralazine
Relative Abundance
Time (min)

Supplemental Table 1.

Percent total MS peak area of parent drug and metabolites from biotransformation experiments with VU238, VU922, or BIBX1382 (5 μM) in hepatic S9 of multiple species (2 mg/mL) in the presence or absence of the XO inhibitor allopurinol (100 μM) or the AO inhibitor hydralazine (50 μM).

		VU238			**VU922 (M1)**		**BIBX1382**		
		VU238	M1	M2	M1	M2	BIBX1382	M1b	M2b
Human	Control	88.8%	11.2%	ND	99.4%	0.6%	22.1%	77.2%	0.7%
	Allopurinol	91.1%	8.9%	ND	99.3%	0.7%	28.5%	71.1%	0.5%
	Hydralazine	100%	ND	ND	>99%	n/d	99.8%	0.2%	ND
Cynomolgus Monkey	Control	43.6%	48.5%	7.9%	70.9%	29.1%	2.1%	78.6%	19.3%
	Allopurinol	51.0%	43.4%	5.7%	76.6%	23.4%	2.7%	82.5%	14.8%
	Hydralazine	100%	ND	ND	100%	ND	100%	ND	ND
Rhesus Monkey	Control	71.4%	26.9%	1.7%	84.6%	15.4%	10.5%	80.2%	9.3%
	Allopurinol	76.9%	22.3%	0.8%	88.8%	11.2%	17.3%	76.5%	6.2%
	Hydralazine	>99%	ND	n/d	>98%	n/d	100%	ND	ND
Rat	Control	41.4%	47.3%	11.3%	70.2%	29.8%	95.4%	1.2%	3.4%
	Allopurinol	44.0%	55.1%	0.9%	96.8%	3.2%	95.8%	1.3%	2.9%
	Hydralazine	>99%	ND	n/d	74.2%	25.8%	100%	ND	ND
Mouse	Control	72.2%	26.1%	1.7%	87.7%	12.3%	97.5%	2.2%	0.3%
	Allopurinol	70.9%	29.1%	ND	99.4%	0.6%	97.6%	2.1%	0.3%
	Hydralazine	>99%	ND	n/d	89.0%	11.0%	100%	ND	ND
Guinea Pig	Control	87.7%	10.7%	1.7%	75.9%	24.1%	71.8%	18.8%	9.4%
	Allopurinol	88.0%	11.1%	0.9%	79.6%	20.4%	72.4%	19.0%	8.5%
	Hydralazine	100%	ND	ND	>98%	n/d	99.9%	0.1%	ND
Minipig	Control	71.2%	28.8%	ND	98.3%	1.7%	5.6%	75.6%	18.8%
	Allopurinol	70.4%	29.6%	ND	98.0%	2.0%	5.2%	75.4%	19.4%
	Hydralazine	100%	ND	ND	>99%	n/d	97.5%	2.5%	ND
Female Cynomolgus Monkey	Control	89.3%	10.7%	ND	95.9%	4.1%	n/a	n/a	n/a
	Allopurinol	92.7%	7.3%	ND	97.1%	2.9%	n/a	n/a	n/a
	Hydralazine	>99%	ND	n/d	>99%	n/d	n/a	n/a	n/a
Female Rat	Control	97.2%	2.8%	ND	83.1%	16.9%	n/a	n/a	n/a
	Allopurinol	96.7%	3.3%	ND	100%	ND	n/a	n/a	n/a
	Hydralazine	>99%	ND	n/d	84.2%	15.8%	n/a	n/a	n/a

ND = not detected

n/d = not determined due to presence of interfering analyte

n/a = no data available

Supplemental Figure 5.

UV chromatograms obtained from extracts of 60-minute incubations with 6-thioxanthine (6-TX, 20 μM) in (A) male cynomolgus monkey hepatic S9 (2 mg/mL), (B) male rat hepatic S9 (2 mg/mL), (C) mixed gender human hepatic S9 (2 mg/mL), (D) male rhesus monkey hepatic S9 (2 mg/mL), (E) male mouse hepatic S9 (2mg/mL), (F) male guinea pig hepatic S9 (2mg/mL), and (G) male minipig hepatic S9 (2mg/mL) demonstrating formation of 6-thiouric acid (6-TUA) in the presence or absence of the XO inhibitor allopurinol (100 μM) or the AO inhibitor hydralazine (50 μM). Chromatograms depicted represent extracted UV plots of spectrum maximums at 340 nm (6-TX) and 354 nm (6-TUA).

LC/UV/MS analysis of 6-TX and 6-TUA. Incubations were carried out as described in the materials and methods section. LC/UV/MS analysis of 6-TX and 6-TUA was performed with an Agilent 1290 Infinity HPLC system coupled to a LTQ XL ion trap mass spectrometer (ThermoFisher Scientific, Waltham, MA). Analytes were separated by gradient elution using a Zorbax Eclipse XDB C18 column (5 μm, 4.6 × 150 mm; Agilent Technologies). Solvent A was 0.1% formic acid in water (pH unadjusted), and solvent B was acetonitrile. The initial mobile phase was held at 95:5 A-B (v/v) for 5.5 minutes and by linear gradient was transitioned to 20:80 A-B over 1.5 minutes, held for 2 minutes, then transitioned back to starting conditions over 0.5 minutes for a total run time of 10 min. The flow rate was 0.800 ml/min. The HPLC eluent was first introduced into an Agilent 1290 diode array detector (spectrum scan 190 – 400 nm) followed by electrospray ionization-assisted introduction into a LTQ XL ion trap mass spectrometer operated in positive ionization mode. Ionization was assisted with sheath and auxiliary gas (ultra-pure nitrogen) set at 50 and 20 psi, respectively. The electrospray voltage was set at 5 kV with the heated ion transfer capillary set at 350 °C and 31 V. Data were analyzed using Thermo XCalibur 2.2 software. LC/UV/MS/MS analysis of analytes identified as 6-TX and 6-TUA are consistent with that of authentic standards of 6-TX and 6-TUA, respectively (data not shown).

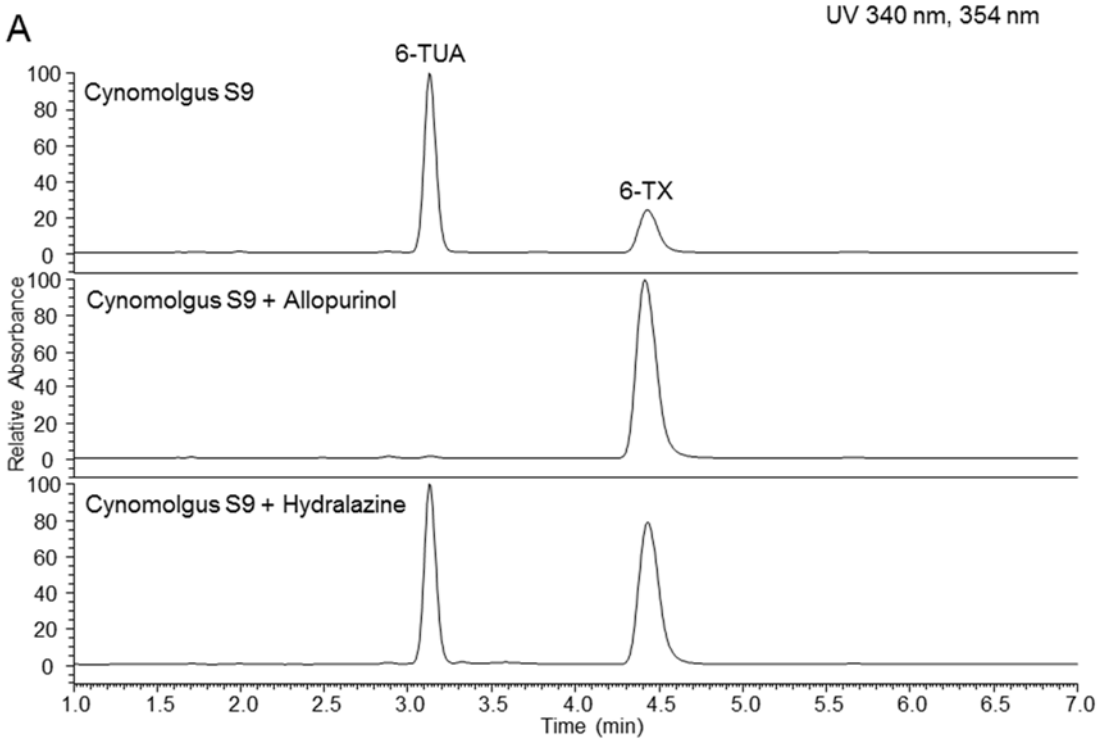

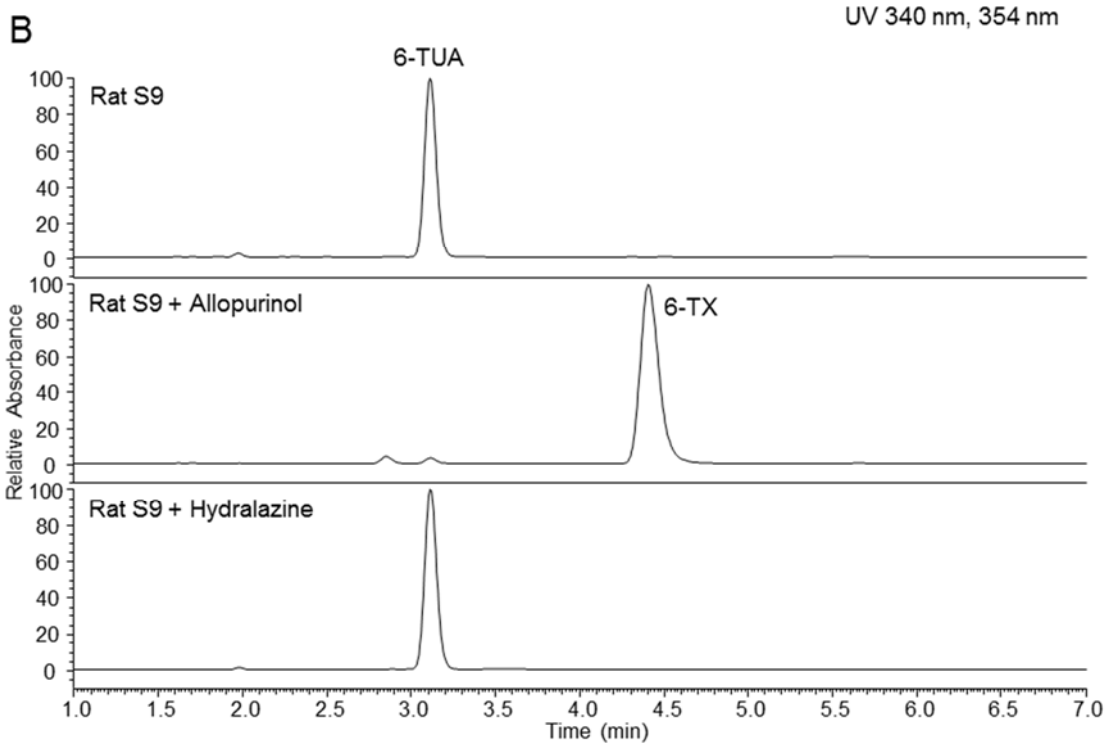
B
UV 340 nm, 354 nm
6-TUA
Rat S9
Rat S9 + Allopurinol
6-TX
Rat S9 + Hydralazine
Relative Absorbance
Time (min)

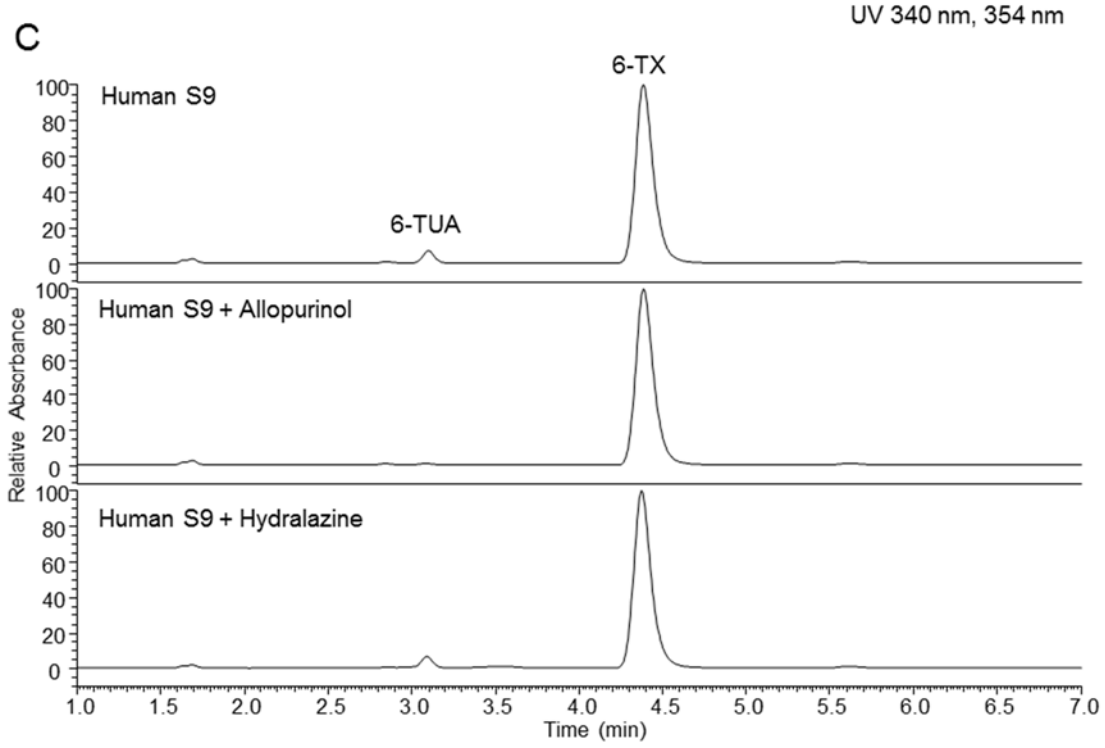
C
UV 340 nm, 354 nm
6-TX
Human S9
6-TUA
Human S9 + Allopurinol
Human S9 + Hydralazine
Relative Absorbance
Time (min)

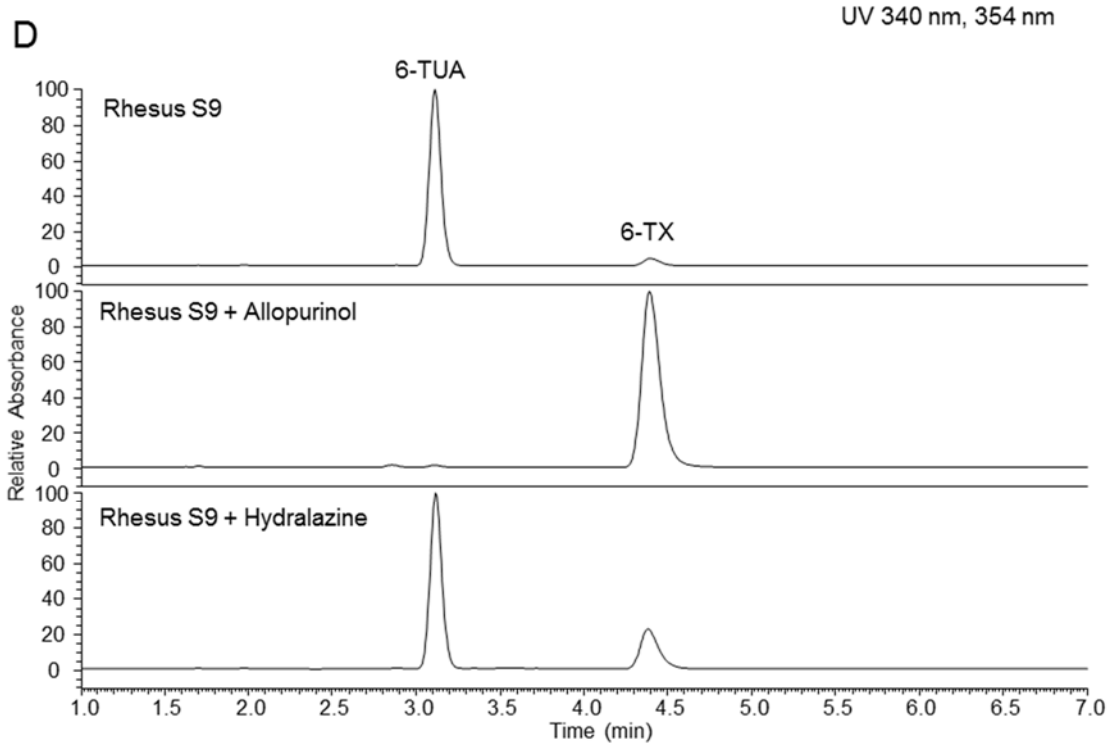
D
UV 340 nm, 354 nm
6-TUA
6-TX
Rhesus S9
Rhesus S9 + Allopurinol
Rhesus S9 + Hydralazine
Relative Absorbance
Time (min)

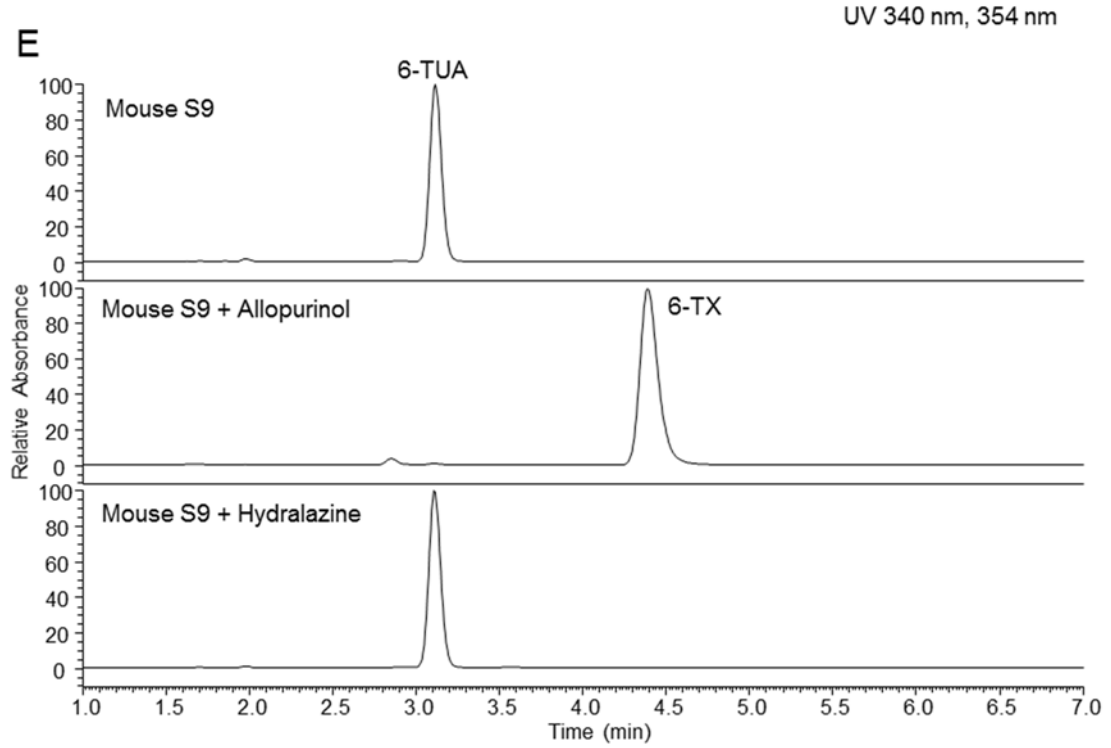
E
UV 340 nm, 354 nm
6-TUA
6-TX
Mouse S9
Mouse S9 + Allopurinol
Mouse S9 + Hydralazine
Relative Absorbance
Time (min)

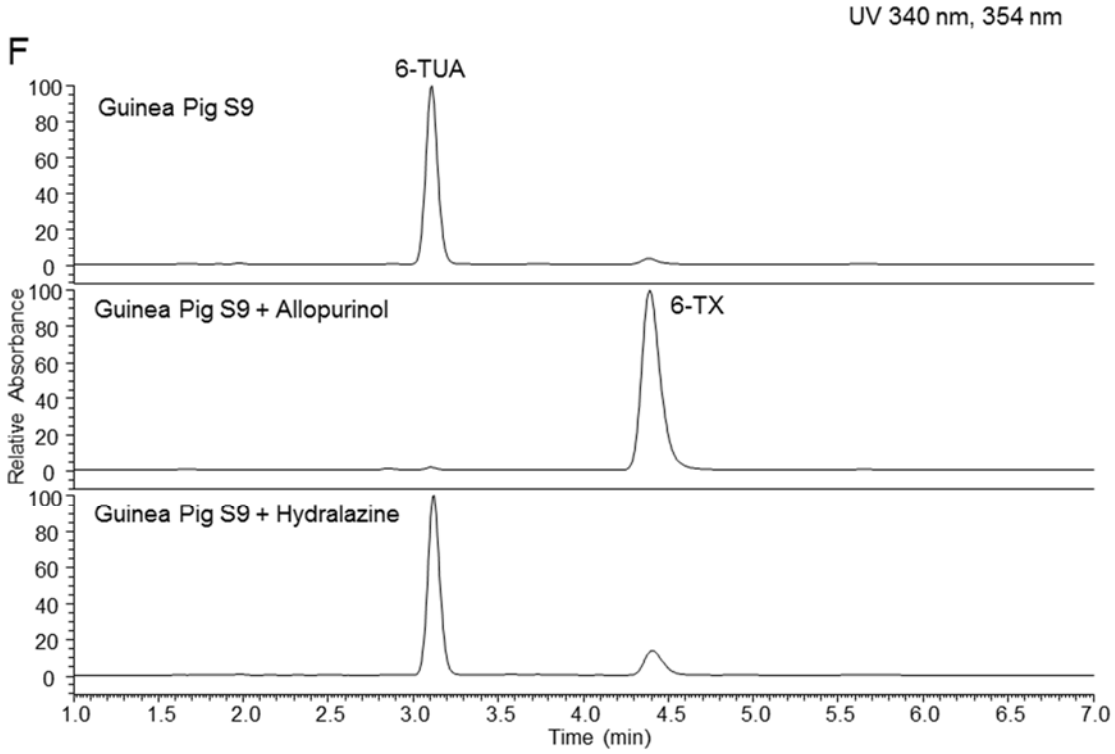
F
UV 340 nm, 354 nm
6-TUA
Guinea Pig S9
Guinea Pig S9 + Allopurinol
6-TX
Guinea Pig S9 + Hydralazine
Relative Absorbance
Time (min)

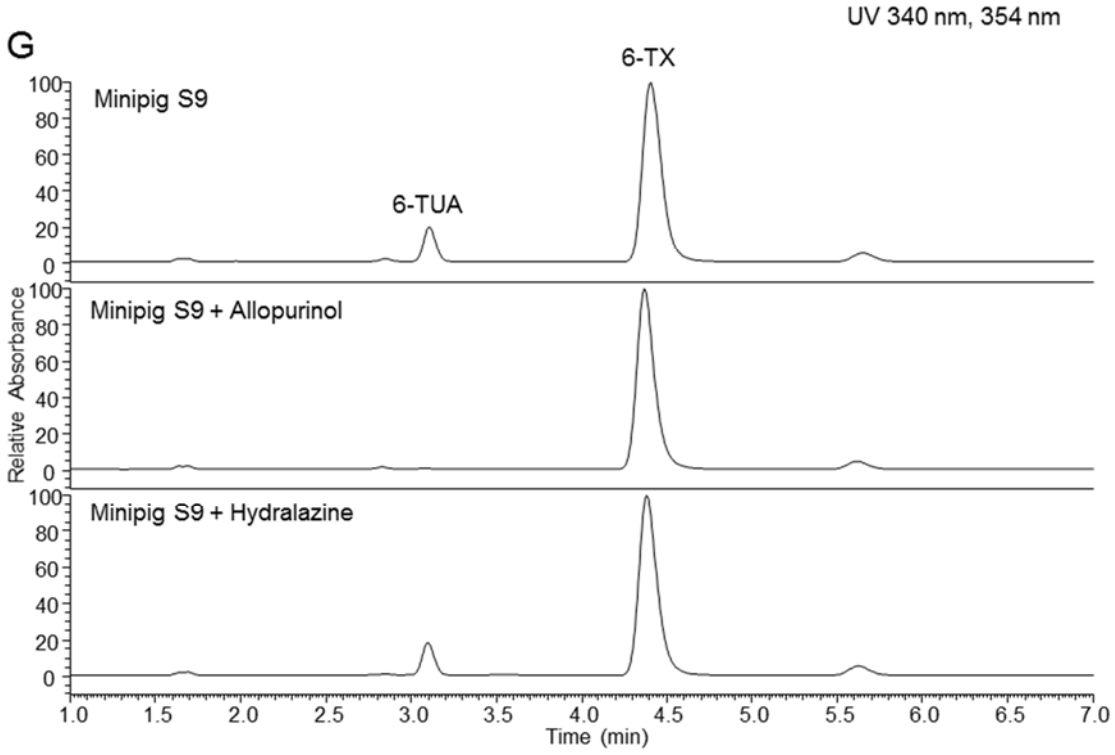
G
UV 340 nm, 354 nm
6-TX
Minipig S9
6-TUA
Minipig S9 + Allopurinol
Minipig S9 + Hydralazine
Relative Absorbance
Time (min)

Supplemental Table 2.

Percent total UV peak area of parent drug (6-TX) and metabolite (6-TUA) from biotransformation experiments (Supplemental Figure 5) with 6-TX (20 μM) in hepatic S9 of multiple species (2 mg/mL) in the presence or absence of the XO inhibitor allopurinol (100 μM) or the AO inhibitor hydralazine (50 μM). 6-TX, 6-thioxanthine; 6-TUA, 6-thiouric acid

		6-TX	6-TUA
Human	Control	95.7%	4.3%
	Allo	99.4%	0.6%
	Hyd	96.1%	3.9%
Cynomolgus	Control	27.5%	72.5%
	Allo	99.3%	0.7%
	Hyd	57.5%	42.5%
Rhesus	Control	5.7%	94.3%
	Allo	99.2%	0.8%
	Hyd	26.1%	73.9%
Rat	Control	ND	100.0%
	Allo	98.2%	1.8%
	Hyd	ND	100.0%
Mouse	Control	ND	100.0%
	Allo	99.6%	0.4%
	Hyd	ND	100.0%
Guinea Pig	Control	4.2%	95.8%
	Allo	99.1%	0.9%
	Hyd	17.6%	82.4%
Minipig	Control	88.9%	11.1%
	Allo	99.7%	0.3%
	Hyd	89.5%	10.5%

ND = not detected